THESIS FOR THE DEGREE OF DOCTOR OF PHILOSOPHY

Filtration of Microcrystalline Cellulose

Electro-assisted filtration and the influence of surface properties

JONAS WETTERLING

Department of Chemistry and Chemical Engineering

CHALMERS UNIVERSITY OF TECHNOLOGY

Gothenburg, Sweden 2017

Filtration of Microcrystalline Cellulose
Electro-assisted filtration and the influence of surface properties
JONAS WETTERLING
ISBN 978-91-7597-578-8

Doktorsavhandlingar vid Chalmers tekniska högskola
Ny serie nr 4259
ISSN 0346-718X

Department of Chemistry and Chemical Engineering
Chalmers University of Technology
SE-412 96 Gothenburg
Sweden
Telephone + 46 (0)31-772 1000

Chalmers Reproservice
Gothenburg, Sweden 2017

Filtration of Microcrystalline Cellulose

Electro-assisted filtration and the influence of surface properties

JONAS WETTERLING

Forest Products and Chemical Engineering
Department of Chemistry and Chemical Engineering
Chalmers University of Technology

ABSTRACT

One of the main requirements for the sustainable usage of materials is the use of renewable resources. This presents the Swedish forestry industry with the promising opportunity of using wood to produce not only traditional paper products but also a range of new materials of high value. The production of new types of materials introduces new challenges: a main one that faces large-scale production processes based on bio-based resources is solid-liquid separation.

Thermal drying is often preceded by a mechanical dewatering technique, such as filtration, in order to achieve an energy-efficient solid-liquid separation. However, conventional pressure filtration operations can be impaired when employed for materials with high specific surface areas due to the operation time and/or equipment size required. This is especially so for materials that form compressible filter cakes. The use of assisted filtration techniques to increase the dewatering rate could therefore play an important role for these types of materials. The application of an electric field during pressure filtration, electro-assisted filtration, is one option to improve the filtration behaviour of materials with charged surfaces.

In this thesis, the filtration behaviour of cellulosic materials with high specific surface areas was studied, and the use of electro-assisted filtration as a method for mechanical dewatering was investigated. The ways in which the surface properties, structure and charge of the solid material affected the filtration behaviour were studied using experimental measurements of the local filtration properties. The local filtration properties were also used to model the pressure filtration operation.

Electro-assisted filtration was shown to increase the filtration rate of the cellulosic material when compared to pressure filtration. The contributions made by electroosmosis and electrophoresis on the filtration operation were described by an electrofiltration model. The specific surface area of the cellulosic material had a large influence on the specific filtration resistance, but was not found to have a major influence on the rate of electroosmotic dewatering. The improvement obtained by electro-assisted filtration thus increased with increasing specific surface area of the solid material.

Keywords: solid-liquid separation, filtration, dead-end filtration, local filtration properties, compressible filter cakes, electro-assisted filtration, electrofiltration, electroosmotic dewatering, modelling

List of publications

This thesis is based on the work contained in the following papers:

I. **Effects of surface structure on the filtration properties of microcrystalline cellulose**
Jonas Wetterling, Tuve Mattsson and Hans Theliander
Separation and Purification Technology 136, 1-9, 2014.

II. **Modelling filtration processes from local filtration properties: The effect of surface properties on microcrystalline cellulose**
Jonas Wetterling, Tuve Mattsson and Hans Theliander
Chemical Engineering Science 165, 14-24, 2017.

III. **Local filtration properties of microcrystalline cellulose: influence of an electric field**
Jonas Wetterling, Tuve Mattsson and Hans Theliander
Submitted.

IV. **The influence of ionic strength on the electro-assisted filtration of microcrystalline cellulose**
Jonas Wetterling, Sandra Jonsson, Tuve Mattsson and Hans Theliander
Manuscript.

V. **The influence of ionic strength on the local filtration properties of titanium dioxide**
Tuve Mattsson, Julie Durruty, Jonas Wetterling and Hans Theliander
Filtration 15(1), 48-57, 2015.

Work related to this thesis has also been presented at the following conferences:

i. Influence of ionic strength on the local filtration properties of TiO_2
Tuve Mattsson, Jonas Wetterling, Julie Durruty and Hans Theliander
Filtech 2013
October 22-24, 2013, Wiesbaden, Germany.

ii. Effect of surface structure on the filtration properties of microcrystalline cellulose
Jonas Wetterling, Tuve Mattsson and Hans Theliander
European Conference on Fluid-Particle Separation, FPS 2014
October 15-17, 2014, Lyon, France.

iii. On the local filtration properties of microcrystalline cellulose
Jonas Wetterling, Tuve Mattsson and Hans Theliander
12th World Filtration Congress, WFC 12
April 11-15, 2016, Taipei, Taiwan.

iv. Electro-assisted filtration of microcrystalline cellulose
Jonas Wetterling, Tuve Mattsson and Hans Theliander
16th Nordic Filtration Symposium
August 24-26, 2016, Lappeenranta, Finland.

v. Influence of the particle surface structure on electro-assisted filtration of microcrystalline cellulose
Jonas Wetterling, Tuve Mattsson and Hans Theliander
Filtech 2016
October 11-13, 2016, Cologne, Germany.

Contribution report

The author of this thesis has made the following contributions to the papers included:

Papers I-III.	Main author. The experiments were planned and the results evaluated under the supervision of Dr. Tuve Mattsson and Prof. Hans Theliander. The author performed the experiments and the modelling work.
Paper IV.	Main author. The study is based on a preliminary experimental study performed by Sandra Jonsson under the supervision of the author. The experiments in the main study were planned and performed by the author, and the results were evaluated together with Sandra Jonsson, Dr. Tuve Mattsson and Prof. Hans Theliander.
Paper V.	Co-author. Active in performing experimental work and in discussing the results. Active in evaluating the experimental data and performing the modelling work. Joint effort made in writing the paper.

Contents

1. Introduction 1
1.1. Background 1
1.1.1. Assisted filtration techniques 2
1.2. Aim 3
1.3. Outline 3
1.4. Wallenberg Wood Science Center 3
2. Theory 5
2.1. Cake filtration 5
2.1.1. Flow through permeable beds 5
2.1.2. Incompressible filter cakes 6
2.1.3. Compressible filter cakes 7
2.2. Local filtration properties 7
2.2.1. Description of local filtration properties 7
2.2.2. Measurement of local filtration properties 11
2.3. Modelling pressure filtration 12
2.3.1. Modelling approaches 12
2.3.2. Filtration model 13
2.4. Electro-assisted filtration 15
2.4.1. Electrokinetic phenomena 15
2.4.2. Electrolysis reactions 17
2.4.3. Ohmic heating 18
2.5. Modelling electrofiltration 19
2.5.1. Electric field strength 19
2.5.2. Governing equations 20
3. Experimental 23
3.1. Filtration equipment 23
3.1.1. Pressure filtration 23
3.1.2. Electro-assisted filtration 24
3.2. Experimental procedure 25
3.2.1. Model materials 25
3.2.2. Characterisation methods 25
3.2.3. Suspension preparation 25

3.2.4. Filtration experiments and filter medium 27
3.3. Material characterisation 27
3.3.1. Microcrystalline cellulose 27
3.3.2. Titanium dioxide 32
4. Results and discussion 35
4.1. Filtration behaviour 35
4.1.1. Influence of the surface structure of particles 35
4.1.2. The influence of particle surface charge 38
4.1.3. Modelling using local filtration properties 41
4.1.4. Summary of pressure filtration results 43
4.2. Electro-assisted dewatering 44
4.2.1. Electroosmotic dewatering 45
4.2.2. Electrofiltration 47
4.2.3. Modelling electro-assisted filtration 55
4.2.4. Summary of the electro-assisted filtration results 58
5. Conclusions 59
6. Future work 61
7. Nomenclature 63
8. Acknowledgements 65
9. References 67

1. Introduction

1.1. Background

Modern society is dependent on having access to a large amount, as well as range, of materials and energy. A main requirement for a sustainable usage of these is that the production originates from renewable resources. However, a large fraction of the demand is currently filled through the usage of fossil resources. Viable renewable alternatives for the production of energy are plentiful: water, solar and wind power are merely a few of the most prominent examples. For production of materials the main renewable sources are bio-based, such as agricultural and forest-based products. A shift towards the production of more materials using biomass as a raw material is therefore desirable, and even necessary, on a global scale.

The forest industry has long been, and remains, one of the most important industries in Sweden. The need for materials produced from renewable resources thus present the Swedish forest industry with promising opportunities: wood could be used as a raw material for production of new materials with a higher value than the traditional use as a construction material or in paper products (van Heiningen, 2006). The concept of a biorefinery, in which the different constituents of wood, or another source of biomass for that matter, are separated and used to produce a range of different products has therefore become a focus of research efforts in the last few decades (Ragauskas *et al.*, 2006). The main constituents of a wood-based raw material are cellulose, lignin and hemicellulose; a number of different applications have been suggested, such as lignin-based carbon fibres (Kadla *et al.*, 2002), commodity chemicals and fuels (Ragauskas *et al.*, 2006).

The use of wood-based cellulose as a raw material in production of materials with high specific surface areas, such as microfibrillated cellulose and cellulose nanocrystals, is one area that has gathered significant research interest. This type of material combines a high mechanical strength and toughness with biodegradability and a low density (Siró and Plackett, 2010). The potential applications of nano-scale cellulosic materials are therefore wide in range: they include films, hydrogels, foams, aerogels and as a component in composite materials (Isogai, 2013). However, scaling up from laboratory scale to production on a commercial level requires process development in order to obtain methods of production that are industrially viable (Oksman *et al.*, 2016). One of the main challenges of scaling up the production of materials with a high specific surface area is to obtain an energy-efficient solid-liquid separation.

In order to achieve an energy-efficient solid-liquid separation, thermal drying is often preceded by a mechanical dewatering technique such as filtration. Mechanical dewatering through

conventional pressure filtration may pose a challenge in the production of materials with high specific surface areas due to high filtration resistances. In the case of materials forming compressible filter cakes, as bio-based materials tend to do, this challenge becomes even more pronounced. The operation time and/or equipment size required can thus be infeasible for production on a commercial scale. The lack of efficient methods for mechanical dewatering increases, in effect, the amount of energy required for thermal drying, and also possibly has a prohibitive effect on the economy of the process. Assisted filtration techniques could, however, be used to facilitate mechanical dewatering and improve the dewatering rate. The extent of mechanical dewatering could therefore be increased which, in turn, would reduce the extent of energy-intensive thermal drying required (Mahmoud *et al.*, 2011).

1.1.1. Assisted filtration techniques

The use of assisted filtration techniques has the potential to play an important role in the production of materials with high specific surface areas by increasing both the dewatering rate and the extent of mechanical dewatering obtained. Depending on the application, assisted filtration techniques have been suggested that use either thermal effects (Clayton *et al.*, 2006), magnetic fields (Stolarski *et al.*, 2006), acoustic fields (Muralidhara *et al.*, 1985; Smythe and Wakeman, 2000), electric fields (Barton *et al.*, 1999; Iwata *et al.*, 2013; Mahmoud *et al.*, 2010), or a combination thereof (Tarleton, 1992). For charged particles with high specific surface areas, such as microfibrillated cellulose and cellulose nanocrystals, the use of electric fields to improve the filtration operation is of particular interest: the charged particle surfaces could be used to influence the filtration behaviour and provide a driving force for separation.

Electro-assisted filtration has been shown to have the potential of improving the dewatering of materials such as wastewater sludge (Citeau *et al.*, 2012; Mahmoud *et al.*, 2011; Olivier *et al.*, 2015), biopolymers (Gözke and Posten, 2010; Hofmann *et al.*, 2006; Hofmann and Posten, 2003) and hydrogels (Tanaka *et al.*, 2014). The technique may also be used to improve the dewatering rate during cross-flow filtration at lower solid contents by preventing fouling of the filter medium (Henry *et al.*, 1977; Wakeman and Tarleton, 1987) and to improve washing operations (Kilchherr *et al.*, 2004). The electric field influences the filtration behaviour by utilising the surface charge of the solid material through a combination of electrophoretic and electroosmotic forces. Dead-end electro-assisted filtration has been shown to possess the potential of decreasing the overall energy demand of solid-liquid separation for a number of systems by reducing the need for thermal drying (e.g. Larue *et al.*, 2006; Loginov *et al.*, 2013; Mahmoud *et al.*, 2011).

Although the industrial potential of dead-end electro-assisted filtration has been shown for a variety of materials, large-scale industrial operations remain in the development stage (Citeau *et al.*, 2015). A number of different designs have been proposed to adapt existing industrial technologies to include electro-assisted dewatering, including filter presses (Kondo *et al.*, 1991), drum filters (Yamaguchi *et al.*, 1993) and belt filters (Jones and Lamont-Black, 2012; Miller *et al.*, 2005). Equipment design where contamination of the filter cake from electrolysis reactions is prevented, e.g. flushing of the electrodes (Hofmann et al., 2006; Hofmann and

Posten, 2003), has also been suggested. So far, however, commercialisation of electro-assisted filtration processes has been focused largely on dewatering of waste sludges, e.g. CINETIK® Linear Electro-Dewatering (Ovivo) and ELODE® (ACE Korea Incorporation).

1.2. Aim

The aim of this thesis is to investigate the use of electro-assisted filtration as a method for mechanical dewatering of cellulosic materials with high specific surface areas. In order to design dewatering operations based on electro-assisted filtration effectively, the relationships between the properties of the solid material, the suspension conditions, the filtration behaviour and the effect of an applied electric field must be established. The work performed in this thesis investigates the behaviour of the solid-liquid separation that occurs in pressure filtration as well as in electro-assisted filtration.

1.3. Outline

The theoretical background to the work included in this thesis is given in Chapter 2. An introduction to cake filtration and the use of local filtration properties are given, along with an introduction to electrokinetic phenomena and electro-assisted filtration. Modelling of filtration operations, both with and without the application of an electric field, is also discussed. The experimental equipment and methods used are described in Chapter 3, as well as a characterisation of the model materials used: microcrystalline cellulose for cellulosic particles with a high specific surface area.

The results are reported in Chapter 4. The influence of the structure and charge of particle surfaces on the behaviour of dead-end filtration is investigated Section 4.1. The resulting effect on the filtration behaviour is described using a filtration model based on measurements of the local filtration properties. The use of electro-assisted dewatering is discussed in Section 4.2 with regards to the properties of cellulose particles and the conditions of the suspension; a filtration model is used to describe the effect of the electric field. The main conclusions are presented in Chapter 5, whilst suggestions for future work are found in Chapter 6.

1.4. Wallenberg Wood Science Center

The research presented in this thesis has been performed within the Wallenberg Wood Science Center. The mission of the research collaboration is to *"create knowledge and competence prerequisites for an innovative industrial value-creation of forest raw material"*. Research undertaken at the Wallenberg Wood Science Center is aimed at developing new materials as well as the process technology required to produce these materials on an industrial scale.

2. Theory

2.1. Cake filtration

Dead-end filtration involves a pressure being applied to a suspension towards a filter medium. The fluid phase passes through the filter medium whilst the solid material is retained and forms a cake structure: the process is therefore often referred to as cake filtration. As the filtration operation progresses, the filter cake grows as solid material is retained. The fluid phase thus flows through both the filter medium and the filter cake being formed. The filtration operation is thus twofold: the flow of fluid through the permeable structure of the cake and the build-up of the filter cake itself must both be described.

2.1.1. Flow through permeable beds

The solid content of the filter cake is described by the solidosity, ϕ, which is defined according to Equation (2.1):

$$\phi = \frac{V_{solid}}{V_{total}} \tag{2.1}$$

where V_{solid} is the volume of solid material in the cake and V_{total} the total volume of the filter cake.

A fluid flowing through the porous structure of the cake subjects the solid particles of which it is comprised to drag forces. The filter cake thus introduces a flow resistance, which gives rise to a pressure drop. The flow rate through a porous bed can be related to this pressure drop by the Darcy equation (Darcy, 1856), commonly written as:

$$u = -\frac{1}{A}\frac{dV}{dt} = -\frac{K}{\mu}\frac{dP_l}{dz} \tag{2.2}$$

where u is the superficial fluid velocity relative to the solid material (in the z-direction, away from the filter medium and into the filter cake), A the flow area, V the volume of the permeate, t the time, K the permeability of the bed, μ the viscosity of the fluid, P_l the hydrostatic pressure and z the distance from the filter medium.

In cake filtration, permeability is often discussed in terms of the resistance to flow. The specific filtration resistance of the filter cake, α, is calculated from its permeability and solidosity according to Equation (2.3) thus:

$$\alpha = \frac{1}{K\rho_s\phi} \tag{2.3}$$

where ρ_s is the density of the solid material.

The drag forces experienced by the solid particles during filtration are accumulated in the cake structure, resulting in a compressive pressure, P_s, that increases in the direction of flow. For a one-dimensional flow, the increase in solid pressure can be related to the hydrostatic pressure through Equation (2.4), assuming that the compressive stress is transmitted through point contact between particles (Tiller, 1953):

$$dP_l + dP_s = 0 \tag{2.4}$$

2.1.2. Incompressible filter cakes

The specific filtration resistance and the solidosity are both constant throughout the structure if the filter cake is assumed to be incompressible. The total flow resistance of the filter cake can then be derived from Equation (2.2). If the filter cake and the filter medium are considered as being two separate resistances in a series, The total pressure drop over the filter cake and the filter medium, ΔP, can then be described by Equation (2.5):

$$\Delta P = (R_c + R_m)\mu\frac{1}{A}\frac{dV}{dt} \tag{2.5}$$

where R_c and R_m are the flow resistances of the filter cake and filter medium, respectively. For incompressible filter cakes, the cake resistance can be described by Equation (2.6):

$$R_c = \int_0^h \frac{1}{K}dh = \alpha_{avg}\phi_{avg}\rho_s h \tag{2.6}$$

where α_{avg} is the average specific filtration resistance, ϕ_{avg} the average solidosity and h the height of the filter cake. Combining Equations (2.5) and (2.6) results in the classical filtration equation given in Equation (2.7) (Ruth, 1935):

$$\frac{dt}{dV} = \frac{\mu\left(\alpha_{avg}cV + R_mA\right)}{A^2\Delta P} \tag{2.7}$$

where c denotes the mass of solids per volume unit of filtrate. This parameter is constant provided that the solid content of the suspensions remains unchanged and the growth of the cake is solely an effect of filtration.

2.1.3. Compressible filter cakes

Most materials do not form incompressible filter cakes. Most filter cakes are, in fact, more or less compressible as a result of rearrangement of particles, breakage of inter-particle structures and/or deformation of particles. As a filter cake is being compressed, the solid material within it has a velocity: v_{solid}. This velocity can be included in Equation (2.2) by using the relative fluid velocity (Shirato *et al.*, 1969):

$$u = v - \left(\frac{1-\phi}{\phi}\right) v_{solid} \tag{2.8}$$

where v is the superficial fluid velocity.

The local filtration properties of compressible filter cakes are dependent on the local compressive pressure and are therefore not constant over the height of the filter cake (Tiller and Cooper, 1960). The formation of compressible filter cakes can therefore result in a filter cake with a high solidosity and a high specific filtration resistance close to the filter medium, where the compressive pressure is high. Increasing the filtration pressure applied may result in further compression of the filter cake's structure which can increase the filtration resistance. The compression thus counteract the flow through the filter cake; increasing the filtration pressure applied may thus not have a major influence on the filtrate flow rate.

Should local measurements of the filter cake's solidosity and the hydrostatic pressure profile be available, then the filtration properties in the filter cake's structure locally may be evaluated locally. A general expression of the local specific filtration resistance can then be obtained by combining Equations (2.2) and (2.3):

$$\alpha = -\frac{1}{u\mu\rho_s\phi}\frac{dP_l}{dz} \tag{2.9}$$

The average specific filtration resistance of a filter cake can then be calculated directly from the local filtration properties using the definition of the average specific filtration resistance in Equation (2.10):

$$\frac{1}{\alpha_{avg}} \equiv \frac{1}{\Delta P_c}\int_0^{P_c}\frac{1}{\alpha}dP_s \tag{2.10}$$

where ΔP_c is the pressure drop over the filter cake.

2.2. Local filtration properties

2.2.1. Description of local filtration properties

2.2.1.1. Empirical relationships

The local solidosity and the local specific filtration resistance of compressible filter cakes increase with the local compressive pressure in the structure of the cake. The pressure

dependencies are often described by empirical relationships (e.g. Tiller, 1955). Several different empirical equations have been used to do describe these relationships (Sedin *et al.*, 2003), one such set of empirical equations is given below (Tiller and Leu, 1980):

$$\phi = \phi_0 \left(1 + \frac{P_s}{P_a}\right)^{\beta} \tag{2.11}$$

$$\alpha = \alpha_0 \left(1 + \frac{P_s}{P_a}\right)^{n} \tag{2.12}$$

where P_a, β and n are empirical parameters. The two parameters ϕ_0 and α_0 can be interpreted as the local solidosity and the local specific filtration resistance, respectively, at the top of the filter cake where no compressible pressure has accumulated in the solid structure.

The solidosity of the filter cake at zero compressible pressure may be estimated as the average solidosity after sedimentation: this gives a reasonable estimation for systems wherein the compressible pressure in the sediment is low compared to the pressure applied during filtration experiments. Another approach, applicable to systems were formation of a network structure prevents settling, is to estimate ϕ_0 as the solid content of the suspension: such a system is thus described as lacking a clear transition between the filter cake and the suspension.

2.2.1.2. Permeability relationships

Empirical relationships are useful tools for describing the pressure dependence of the local filtration properties. This approach does not, however, have the ability to predict how altered material properties affect filtration behaviour. Several approaches attempt to describe the relationship between the specific filtration resistance and the filter cake solidosity in terms of particle properties; a selection of them are presented in the sections that follow.

2.2.1.2.1. The Kozeny-Carman equation

A classical approach to describing the permeability of a porous medium is to use the Kozeny-Carman equation. If the porous medium is considered as being an assembly of capillary pores, with a uniform size and geometry, then the corresponding pressure drop for laminar flow of an incompressible fluid can be determined from the Hagen-Poiseuille equation thus:

$$-\frac{dP_l}{dz} = \frac{32\mu v_{cap}}{D_{cap}^2} \tag{2.13}$$

where v_{cap} is the average velocity of the fluid in the pores and D_{cap} the hydraulic diameter of a pore. By assuming flow in cylindrical capillaries, these parameters can be related to the local filter cake solidosity and the superficial fluid velocity through Equations (2.14) and (2.15):

$$v_{cap} = \frac{u}{1 - \phi} \tag{2.14}$$

$$D_{cap} = \frac{4(1 - \phi)}{S_p \phi} \tag{2.15}$$

where S_p denotes the specific surface area of the solid material. Combining Equations (2.2) and (2.13) gives the Kozeny-Carman equation (Carman, 1937; Kozeny, 1927):

$$K = \frac{(1-\phi)^3}{k S_p^2 \phi^2} \tag{2.16}$$

where the empirical parameter k is known as the "Kozeny-Carman constant". This can be considered a correction factor that adjusts for the shape and tortuosity of the capillary pores. The value of the Kozeny-Carman constant has been found to be dependent on the shape of the particles that constitute the porous medium as well as the solidosity of the bed (Coulson, 1949). A value between 4.8 and 5 is generally used to describe the flow through beds with mono-sized spheres (Carman, 1937; Happel, 1958; Tien and Ramarao, 2013).

The Kozeny-Carman equation can be used to describe the relationship between solidosity and permeability for flow through beds of solid particles. The approach is however insufficient for porous particles, as the flow behaviour may differ significantly between the interior and exterior of the particles. The equation can be modified for flow through beds composed of porous particles with negligible permeability to include the solidosity of the particles, ϕ_i:

$$K = \frac{(1-\phi/\phi_i)^3}{k S_{p,ext}^2 (\phi/\phi_i)^2} \tag{2.17}$$

where $S_{p,ext}$ is the specific external surface area of the porous particles.

2.2.1.2.2. The impermeable sphere model

The relationship between permeability and solidosity can also be described as flow around individual particles. A cell model proposed by Happel (1958) can be used to calculate the permeability of a system described by a solid spherical particle in a concentric spherical fluid cell. The dimension of the fluid cell is set so that the solidosity of the system corresponds to the local solidosity of the filter cake. The boundary conditions of the model are no-slip at the interface between the particle and the cell, and no tangential stress at the outer boundary of the cell. The permeability can then be described by Equation (2.18) for creeping flow:

$$K = \frac{a^2}{3\gamma^3} \frac{2 - 3\gamma + 3\gamma^5 - 2\gamma^6}{3 + 2\gamma^5} \tag{2.18}$$

where a denotes the radius of the inner sphere and γ describes the fraction of the cell volume that is unavailable for flow, as given by Equation (2.19):

$$\gamma^3 = (a/b)^3 = \phi/\phi_i \tag{2.19}$$

where b denotes the cell radius. The impermeable sphere model as published by Happel assumed the inner sphere to be solid, i.e. ϕ_i = 1. A modified version that accounts for the solidosity of the particle, as described in Equation (2.19), can be used to describe flow around porous particles with negligible permeability.

2.2.1.2.3. The permeable sphere model

The boundary conditions in the impermeable sphere model described in Section 2.2.1.2.2 can be changed to include the permeability of the inner sphere. The permeable sphere model can then be used to describe flow both around and through permeable particles or agglomerates. Deo (2009) described flow through the inner sphere by the Brinkman equation (Brinkman, 1947) and assumed velocity and stress components to be continuous at the interface between the particle and the fluid cell. The permeability of the system could then be described by Equation (2.20):

$$K = \frac{2a^2\left(1+\frac{3}{2}\{k_1-\gamma+(1+14k_1+30k_1^2)\gamma^5\}\right)}{9\gamma^3\left(1+\frac{2}{3}\gamma^5+10\gamma^5\left(k_1-\frac{1}{3}\lambda\right)\right)} + \frac{2a^2(\lambda\{1-3(2+5k_1)\gamma^5+5\gamma^6\}-(1+15k_1)\gamma^6)}{9\gamma^3\left(1+\frac{2}{3}\gamma^5+10\gamma^5\left(k_1-\frac{1}{3}\lambda\right)\right)} \tag{2.20}$$

in which γ, λ and k_1 are given by Equations (2.19), (2.21) and (2.22), respectively.

$$\lambda = \frac{\sinh\left(\frac{1}{\sqrt{k_1}}\right)}{\frac{1}{\sqrt{k_1}}\cosh\left(\frac{1}{\sqrt{k_1}}\right)-\sinh\left(\frac{1}{\sqrt{k_1}}\right)} \tag{2.21}$$

$$k_1 = k_i/a^2 \tag{2.22}$$

where k_i is the permeability of the inner sphere. The permeability of the inner sphere can be used as a model parameter directly or, alternatively, the permeable sphere model can be coupled with e.g. the Kozeny-Carman equation to estimate the permeability the inner sphere:

$$k_i = \frac{(1-\phi_i)^3}{\kappa S_{p,i}^2 \phi_i^2} \tag{2.23}$$

where $S_{p,i}$ is the specific internal surface area of the particle.

2.2.2. Measurement of local filtration properties

2.2.2.1. Compression-permeability cell

The relationship between solidosity, permeability and compressive pressure has traditionally been determined using the compression-permeability cell (Ruth, 1946). A cake of uniform solidosity is formed at a specified compressive pressure and the fluid flow through the cake is measured, allowing the permeability to be calculated using the Darcy equation. The technique thus allows calculation of local filtration properties to be made from average measurements under the assumption that a homogeneous cake has been formed (Grace, 1953). Either a filter cake is formed for each applied pressure investigated (Teoh *et al.*, 2002) or the pressure applied to a filter cake can be increased during measurement to determine the pressure dependence (Iritani *et al.*, 2006).

Obtaining a uniform cake is, however, problematic due to friction between the cake and the cell wall (Tiller *et al.*, 1972). Several attempts have therefore been made to correct the local applied pressure in compression-permeability cells (Shirato *et al.*, 1968; Tiller and Lu, 1972).The use of compression-permeability cell measurements to determine local filtration properties has also been questioned with respect to possible time dependence of the cake's structure (Wakeman, 1978).

2.2.2.2. Local pressure measurements

The local hydrostatic pressure in a filter cake can be measured by inserting pressure probes into the filtration cell: several different configurations of pressure probes have been used in previous studies (Fathi-Najafi and Theliander, 1995; Johansson and Theliander, 2003; Okamura and Shirato, 1955; Rietema, 1953; Shirato *et al.*, 1971). The design must be chosen so that the effects on measurements from friction at the outer filter cell wall and disturbance to the formation of the filter cake or the suspension flow are minimised. The compressive pressure in the filter cake's structure can be obtained from the local hydrostatic pressure, assuming that the sum of the local hydrostatic pressure and the local solid compressive pressure equals the filtration pressure applied, see Equation (2.4).

2.2.2.3. Local solidosity measurements

2.2.2.3.1. Cake dissection

The classical approach to studying the local solidosity of filter cakes is to dissect the cake that is formed cake (Dell and Sinha, 1964; Meeten, 1993; Yim and Song, 2008; Young, 1911). The filtration experiment is halted, and the cake is collected and requires physical division of layers that are analysed separately. Apart from local solidosity measurements, the method may also be used to measure variations in e.g. particle size distribution across the filter cake. The destructive nature of the method does, however, require a large number of filtration experiments in order to obtain a time resolution. A possible modification to the dissection method that avoids the destruction of the cake is to use the cake colouration (Hutto, 1957) method, which feeds the

filtration process with coloured suspensions. This allows the local solidosity of the filter cake to be calculated from the height of the coloured bands observed within it.

2.2.2.3.2. Electrical conductivity

A non-destructive method for measuring the local solidosity of filter cakes is to use the local electrical conductivity (Chase and Willis, 1992; Holdich and Sinclair, 1992; Rietema, 1953; Shirato *et al.*, 1971; Wakeman, 1981). Electrodes are placed in the filter cell and the voltage is recorded during the filtration process. The relationship between the electrical conductivity and the solidosity of a filter cake can then be determined by calibrating the conductivity measurement with that of known solidosities of filter cakes.

2.2.2.3.3. Radiation attenuation

A less intrusive method for measuring the solidosity of a filter cake is through the usage of radiation attenuation. Radiation passing through the filter cake in question is measured: the difference in the attenuation coefficients of the solid material and the fluid phase is then used to calculate the local solidosity. The attenuation of x-rays (Auzerais *et al.*, 1990; Bierck *et al.*, 1988; Shen *et al.*, 1994; Tiller *et al.*, 1995) and γ-radiation (Bergström, 1992; Johansson and Theliander, 2003) has been used to study local solidosity during both filtration and sedimentation experiments. The experimental error of the local solidosity calculated from radiation attenuation measurements is largely dependent on three factors, namely the source of radiation, the absolute and relative attenuation coefficients of the solid material and the fluid, and the sampling time used for the measurements. A strong source of radiation and a large difference in the radiation attenuation between the phases thus allow for a better time resolution.

2.2.2.3.4. Nuclear magnetic resonance

The solidosity profile can also be measured non-destructively using the nuclear magnetic resonance (NMR) technique, which has the added advantage of distinguishing between free water and water that is bound either physically or chemically (Kopinga and Pel, 1994). It has been used to measure local solidosity during filtration in a number of studies (Dirckx *et al.*, 2000; Horsfield *et al.*, 1989; La Heij *et al.*, 1996; Saveyn *et al.*, 2006).

2.3. Modelling pressure filtration

2.3.1. Modelling approaches

A number of different approaches have been used to describe the flow through growing filter cakes by combining the Darcy equation with the continuity equation: using either spatial co-ordinates (e.g. Smiles and Kirby, 1987; Tien and Bai, 2003; Wakeman, 1978) or material co-ordinates (e.g. Atsumi and Akiyama, 1975; Sørensen *et al.*, 1996). The relation between the compressive pressure and the solidosity of a filter cake is required nevertheless, and is often

described in filtration models with empirical relationships (Atsumi and Akiyama, 1975; Smiles, 1970; Tosun, 1986; Wakeman, 1978). Similarly, the relation between the permeability and solidosity of a filter cake can be described either by empiricism or by one of the permeability relationships given in Section 2.2.1.2.

The influence of interactions between particles on the compressibility of a filter cake has been modelled for non-agglomerating particles in the colloidal size range (Bowen and Jenner, 1995). The compressive pressure in the cake's structure is assumed to equal the sum of the interparticle forces according to DLVO theory. The solidosity of the filter cake is then estimated using the interparticle spacing and assumes a closely-packed geometry. Another approach has been suggested to account for the additional formation of structure in agglomerating systems (Koenders *et al.*, 2000; Koenders and Wakeman, 1997): a model where the compressive pressure is balanced by the stiffness of the cake, which is dependent on the solidosity of the filter cake as well as the double layer forces. Numerical simulations using DLVO theory to describe the effect of electrostatic particle interactions on the formation of a filter cake have also been performed (e.g. Fu and Dempsey, 1998; Schäfer *et al.*, 2010).

Modelling can also be performed in terms of compressional rheology (Buscall and White, 1987) that has been applied to describe filtration behaviour (e.g. Landman *et al.*, 1991; Landman and White, 1997; Stickland *et al.*, 2006). In compressional rheology, the stability of the filter cake's structure is described by the yield stress of the network, whereas the drag between the solid and fluid phases is described by a hydrodynamic interaction parameter. The yield stress and the hydrodynamic interaction parameter can both be obtained from experimental measurements, and the solidosity dependences of the parameters can be described by empirical relationships (Buscall and White, 1987; Landman and White, 1992; Landman *et al.*, 1995; Stickland and Buscall, 2009).

2.3.2. Filtration model

The modelling approach used to describe the filtration operation in this thesis is described in the following section. The model describes the growing filter cake in spatial co-ordinates; the relationships between the compressive pressure, filter cake solidosity and cake permeability were determined from measurements of the local filtration properties.

2.3.2.1. Governing equations

The continuity equations for the solid material and the fluid in the filter cake, expressed in spatial co-ordinates, are given by Equations (2.24) and (2.25):

$$\frac{\partial \phi}{\partial t} = \frac{\partial v}{\partial z} \tag{2.24}$$

$$\frac{\partial v}{\partial z} = -\frac{\partial v_{solid}}{\partial z} \tag{2.25}$$

The superficial velocities of the fluid, v, and the solid material, v_{solid}, are related to the permeability of the filter cake and the local pressure drop by the modified Darcy equation given in Equation (2.26):

$$v - \frac{1-\phi}{\phi} v_{solid} = -\frac{K}{\mu}\frac{dP_l}{dz} \tag{2.26}$$

For systems with an incompressible fluid phase and an incompressible solid material, a local mass balance states that the sum of the superficial fluid velocities is constant throughout the filter cake. As the solid material is stationary at interface between the filter medium and the filter cake, Equation (2.27) is valid at all distances from the filter medium during the filtration operation:

$$v + v_{solid} = -\left(\frac{K}{\mu}\frac{dP_l}{dz}\right)_{z=0} \tag{2.27}$$

Combining Equations (2.26) and (2.27) allows the continuity equation given in Equation (2.24) to be expressed as Equation (2.28) (Wakeman, 1978):

$$\frac{\partial \phi}{\partial t} = \frac{\partial v}{\partial z} = -\frac{d}{dz}\left[\phi\left(\frac{K}{\mu}\frac{dP_l}{dz}\right)\right] + \left(\frac{K}{\mu}\frac{dP_l}{dz}\right)_{z=0}\frac{\partial \phi}{\partial z} \tag{2.28}$$

The local permeability of the filter cake can be described by one of the permeability relationships given in Section 2.2.1.2. Using the approach described in Section 2.2.1.2.2, the modelling work used in this thesis described the solid material as impermeable porous spheres. The local solidosity of the filter cake was described as a function of the solid compressive pressure in the filter cake by the empirical relationship given in Equation (2.11).

2.3.2.2. Boundary conditions

The position of the interface between the filter cake and the suspension moves continually during the filtration operation as the filter cake grows. This growth is given by the filtrate flow and a mass balance of the filter cake:

$$\frac{dh}{dt} = -u(z=0)\frac{\phi_s}{\phi_{avg}(t) - \phi_s} \tag{2.29}$$

where h is the height of the filter cake, ϕ_s the solidosity of the suspension and $\phi_{avg}(t)$ the time-dependent average solidosity of the filter cake.

The solid compressive pressure at the top of the filter cake is assumed to be zero. The local hydrostatic pressure at the boundary is thus:

$$P_l(z=h) = P_{applied} \tag{2.30}$$

where $P_{applied}$ is the applied filtration pressure.

The local hydrostatic pressure at the interface between the filter cake and the filter medium is dependent on the filter medium resistance as well as the filtrate flow rate:

$$P_l(z = 0) = -\mu R_m u(z = 0) \tag{2.31}$$

2.3.2.3. Numerical solution method

The governing equations were solved, subject to the boundary conditions, using COMSOL Multiphysics® V.5.2. The system was set up as a one-dimensional problem with an expanding mesh. The modelling was performed under the assumption that the filter cake had an initial height of 10 μm at the start of the filtration operation.

2.4. Electro-assisted filtration

Electrofiltration is an assisted filtration technique that uses an electric field to influence the filtration behaviour. Charged colloidal particles move in an electric field through electrophoresis; the electric field that is applied may therefore influence the growth of the filter cake during electro-assisted filtration (Moulik, 1971). The electric field also gives an electroosmotic flow, resulting in an additional driving force for separation (Kobayashi *et al.*, 1979; Yukawa *et al.*, 1971; Yukawa *et al.*, 1976). In addition to electrophoresis and electroosmosis, the electric field also causes electrolysis reactions at the electrodes as well as a temperature rise in the filter cell due to ohmic heating. A brief introduction to the various effects of an electric field applied during electro-assisted filtration is given in the following sections.

2.4.1. Electrokinetic phenomena

2.4.1.1. Electrophoresis

A charged particle in an electric field experiences a force in the direction of the oppositely charged electrode. Such a particle accelerates until either the electric force is balanced by the viscous resistance of the fluid phase or it is constrained mechanically by e.g. a filter medium or a filter cake structure. If this particle is of sufficient size that its curvature is negligible (i.e. the surface is considered to be planar), the electrophoretic velocity of a non-conducting solid particle is given by the Helmholtz-Smoluchowski equation (Hiemenz and Rajagopalan, 1997) as:

$$v_e = \frac{\varepsilon_{rs}\varepsilon_0\zeta}{\mu}E \tag{2.32}$$

where v_e is the electrophoretic velocity in the direction towards the cathode, ε_{rs} the relative dielectric constant of the fluid, ε_0 the permittivity of vacuum, ζ the zeta-potential of the solid material and E the strength of the electric field.

Equation (2.32) is valid for any particle geometry provided that the radius of curvature is large compared to the Debye length, κ^{-1}, i.e. $a\kappa \gg 1$ (Delgado *et al.*, 2007). The Helmholtz-Smoluchowski equation is thus valid for large particles or for systems with a high electrolyte content, as the Debye length is given by Equation (2.33) for monovalent electrolyte system:

$$\kappa^{-1} = \sqrt{\frac{\varepsilon_{rs}\varepsilon_0 k_B T}{2N_A e^2 I_{is}}} \tag{2.33}$$

where k_B is the Boltzmann constant, T the temperature, N_A the Avogadro constant, e the elementary charge and I_{is} the ionic strength of the system.

An alternative way of describing the electrophoretic flow is to consider a non-conducting spherical particle that gives no deformation of the electric field. This behaviour is valid if the particle's radius is small compared to the Debye length, i.e. $a\kappa \ll 1$, and results in the Debye-Hückel equation (Hiemenz and Rajagopalan, 1997):

$$v_e = \frac{2}{3}\frac{\varepsilon_{rs}\varepsilon_0\zeta}{\mu}E \tag{2.34}$$

The expressions of the electrophoretic velocity given in Equations (2.32) and (2.34) describe the limiting cases for electrophoretic velocity for two fundamentally different assumptions valid for particles of different size ranges. The electrophoresis behaviour may also be solved for the transition between these regimes depending on the size and charge of the particles and the electrolyte content of the suspension (Henry, 1931).

2.4.1.2. Electroosmosis

An electric field applied to a stationary charged surface results in a relative motion between the solid and the fluid through electroosmotic flow. Electroosmotic flow arises as ionic components in the electrical double layer are accelerated: this creates viscous forces which cause movement of the bulk fluid. The velocity at the slip plane of the surface is zero, and the electroosmotic flow velocity is the velocity of the bulk liquid away from the electrical double layer. As for the electrophoresis in Section 2.4.1.1, the electroosmotic velocity can be described by the Helmholtz-Smoluchowski equation (Lyklema, 1995):

$$v_{eo} = -\frac{\varepsilon_{rs}\varepsilon_0\zeta}{\mu}E \tag{2.35}$$

where v_{eo} is the electroosmotic velocity of the fluid in the direction towards the cathode. The Helmholtz-Smoluchowski equation is valid when $a\kappa \gg 1$.

For systems consisting of small particles and with low ionic strengths, the conductivity of the electrical double layer (i.e. the surface conductivity) may have a significant influence on the electroosmotic flow. For a cylindrical pore, the contribution made by the surface conductivity to the overall conductivity of the system can be described by (Delgado *et al.*, 2007):

$$K_{sys} = K_L + 2K^{\sigma}/a \tag{2.36}$$

where K_{sys} is the conductivity of the system, K_L the conductivity of the bulk liquid, K^{σ} the surface conductivity and a the radius of the pore. The influence of the surface conduction on the electroosmotic velocity in a cylindrical capillary with an arbitrary radius can be described by (Rice and Whitehead, 1965):

$$v_{eo} = -\frac{\varepsilon_{rs}\varepsilon_0\zeta}{\mu} A_c E[1 - G(\kappa a)] \tag{2.37}$$

where A_c is the cross-sectional area of the capillary, κ^{-1} the Debye length, a the radius of the capillary and $G(\kappa a)$ is defined by:

$$G(\kappa a) = \frac{2I_1(\kappa a)}{\kappa a I_0(\kappa a)} \tag{2.38}$$

where I_0 and I_1 are the zeroth-order and first order modified Bessel functions, respectively, of the first kind.

2.4.1.3. Ion migration

In addition to electrophoresis and electroosmosis, there will also be movement of ions in an electric field. The ion migration velocity can be described by (Yu and Neretnieks, 1996):

$$v_d = \frac{z_i}{|z_i|} u_i E \tag{2.39}$$

where v_d is the drift velocity of electromigration, z_i the charge number and u_i the ionic mobility. The movement of ions in the system during electro-assisted filtration is therefore influenced by a combination of ion migration, electroosmotic flow and fluid flow from the filtration pressure applied (Kilchherr *et al.*, 2004).

2.4.2. Electrolysis reactions

Electrochemical reactions take place at the electrodes when an electric field is applied to a suspension. These reactions are influenced by the material that compose the electrodes as well as by ions in the suspension (Lockhart, 1983a; Mahmoud *et al.*, 2010). The electrochemical reactions at the anode are given by Equations (2.40) and (2.41) for a water-based system:

$$2H_2O \rightarrow O_{2,(g)} + 4H^+ + 4e^- \qquad E_0 = 1.23\ V \tag{2.40}$$

$$M \rightarrow M^{n+} + ne^- \tag{2.41}$$

whereas the electrochemical reactions at the cathode are given by Equations (2.42) and (2.43):

$$2H_2O + 2e^- \rightarrow 2OH^- + H_2 \qquad E_0 = -0.83\,V \tag{2.42}$$

$$M^{n+} + ne^- \rightarrow M \tag{2.43}$$

where M is the electrode material and E_0 is the standard electrode potential of the reaction at 298 K. The electrode material of the anode should be chosen so that its standard electrode potential is higher than that of water electrolysis in order to prevent corrosion. Anodes used for electrofiltration are therefore often either titanium meshes coated by mixed metal oxides (Citeau *et al.*, 2012; Raats *et al.*, 2002) or made of noble metals (Rabie *et al.*, 1994; Saveyn *et al.*, 2006).

The amount of electrolysis reactions at the electrodes is proportional to the intensity of the current according to Faraday's law:

$$n_p = \frac{1}{F}\int I\,dt \tag{2.44}$$

where n_p is the amount of electrolysis products, F the Faraday constant and I the electrical current. The electrolysis reactions result in acidic conditions at the anode and alkaline conditions at the cathode; the resulting electrolysis products are transported by the bulk flow of fluid during electro-assisted filtration. The ionic products formed also migrate in the filter cell due to electromigration, giving a pH profile between the electrodes (Larue and Vorobiev, 2004; Yoshida *et al.*, 1999). The local pH in the filter cake may influence the filtration behaviour during electrofiltration by affecting the surface charge of the particles. The surface charge has a direct influence on the electrokinetic effects (Citeau *et al.*, 2011; Hofmann and Posten, 2003; Wakeman, 1982) and the effect on particle-particle interactions may also influence the specific filtration resistance of the material. The products of the electrolysis reactions can be removed from the system by flushing the electrodes: this approach has been used both on a laboratory scale (Citeau *et al.*, 2016; Hofmann and Posten, 2003; Larue *et al.*, 2006) and pilot scale (Hofmann *et al.*, 2006).

2.4.3. Ohmic heating

Electric power is converted into heat by ohmic heating when an electric current is passed through a conductor (Joule, 1841). Ohmic heating is expressed by:

$$\dot{Q}=I^2R \tag{2.45}$$

where $\dot{Q}$ is the power dissipated by the resistance and R is the electrical resistance of the system.

In the case of electro-assisted filtration operations, the extent of ohmic heating is influenced by the electric field that is applied as well as by the electrical resistance of the suspension. For suspensions with a high ionic strength, the electrical conductivity of the system is high and a higher current density is therefore required to maintain the electric field. The influence of the ionic strength of the suspension on ohmic heating is thus very pronounced. Moreover, ohmic

heating has been shown to have a significant influence on electro-assisted filtration operations through the temperature dependence of the viscosity of water, depending on the process conditions (Curvers *et al.*, 2007; Loginov *et al.*, 2013; Mahmoud *et al.*, 2011; Navab-Daneshmand *et al.*, 2015; Weber and Stahl, 2002).

2.5. Modelling electrofiltration

The modelling of electrofiltration operations is often based on the classical filtration equation, Equation (2.7), with additions accounting for the electrokinetic effects (e.g. Iwata *et al.*, 2013; Mahmoud *et al.*, 2010). The inclusion of an electrophoretic coefficient and an electroosmotic pressure in the filtration equation allow the electrokinetic effects to be described by Equation (2.46) (Yukawa *et al.*, 1976) as:

$$\frac{dV}{dt} = \frac{(\Delta p_H + \Delta p_E)A^2}{\mu\left(\alpha_{avg} c \left(\frac{E_{cr} - E}{E_{cr}}\right) V + R_m\right)} \tag{2.46}$$

where Δp_H is the hydraulic pressure, Δp_E the electroosmotic pressure and E_{cr} the critical electric field strength. Employing a modelling approach that includes the electroosmotic pressure and the electrophoretic coefficient $(E_{cr} - E)/E_{cr}$ results in two model parameters for each filtration condition and applied electric field (e.g. Weber and Stahl, 2002).

Different approaches have been suggested to describe the influence of the applied electric field on the electroosmotic contribution to dewatering (e.g. Iwata *et al.*, 2013). A modelling approach based on the work of Saveyn *et al.* (2005) is used in this work: both the electrophoretic and electroosmotic effects are described using the apparent zeta-potential as the only model parameter for the electrofiltration experiments. The model approach is described in the sections that follow.

2.5.1. Electric field strength

For systems where the electrical properties of the solid material and the fluid differ, the electric field strength is not constant throughout the filter cell. If the solid material is non-conductive, and the surface conductivity is negligible compared to the electrical conductivity of the fluid, then the electric field strength in both the filter cake and the suspension can be related through their respective electrical resistances. The relation between the electric field strengths is then described by:

$$E_c(1 - \phi_c) = E_s(1 - \phi_s) \tag{2.47}$$

where E_c and E_s are the electric field strengths in the filter cake and suspension, respectively, ϕ_c the solidosity of the filter cake and ϕ_s the solidosity of the suspension. The strength of the electric field can be found by considering the filter cake, the suspension above it and the filter medium as being electrical conductors in series:

$$U_{applied} - U_{open} = E_c h + E_s(d - h) + IR_{m,e} \tag{2.48}$$

where $U_{applied}$ is the applied voltage, U_{open} the open circuit voltage, h the height of the filter cake, d the separation between the electrodes and $R_{m,e}$ the electrical resistance of the filter medium. The open circuit voltage of the system used in this thesis was determined as being 5±3 V by measuring the electrical resistance at different applied voltages, and is in the same range reported in previous studies using platinum electrodes (Rabie *et al.*, 1994; Vijh, 1999). The electrical resistance of the filter medium has been shown to have an influence on the power demand of electrofiltration operations (Citeau *et al.*, 2012; Yu *et al.*, 2010), but was not found to be significant for the systems used here.

2.5.2. Governing equations

The electrofiltration process can be described as a combination of filtrate flow generated by the applied filtration pressure and electroosmotic flow. The filtrate generated by the applied filtration pressure can be described by the filtration equation:

$$\frac{dV_p}{dt} = \frac{\Delta p_H A}{\mu\left(\alpha_{avg} c\left(\frac{\phi_c - \phi_s}{\phi_s}\right) h + R_m\right)} \tag{2.49}$$

where V_p is the accumulated filtrate volume and $\alpha_{avg}c$ the average filtration resistance per filtrate volume. The values of $\alpha_{avg}c$, R_m and the average cake solidosity ϕ_c were determined from pressure filtration experiments without the application of an electric field. Modelling the local filtration properties of microcrystalline cellulose shows that the average filter cake solidosity and the average specific filtration resistance remain fairly constant throughout the filtration operation, even though the filter cake that is formed is compressible (Mattsson *et al.*, 2012; Wetterling *et al.*, 2017). The electrofiltration model can therefore be expected to describe the overall filtration behaviour despite the fact that the use of a constant filter cake solidosity will underestimate the solidosity and the pressure drop in the region close to the filter medium.

The rate of electroosmotic flow obtained at the cathode during the electrofiltration experiments is described by the Helmholtz-Smoluchowski equation:

$$\frac{dV_{eo}}{dt} = -\frac{\varepsilon_{rs}\varepsilon_0\zeta}{\mu} E_c(1 - \phi_c)A \tag{2.50}$$

where the apparent zeta-potential, ζ, is used as a model parameter. The filtrate flow rate during the electrofiltration process can then be described as a combination of the filtrate generated by the applied filtration pressure, V_p, and the filtrate resulting from electroosmotic flow, V_{eo}. The total filtrate volume is therefore given by:

$$V = V_p + V_{eo} \tag{2.51}$$

The growth of the filter cake is determined by a mass balance between the particles deposited on the filter cake from the flow of filtrate and the electrophoretic transport of solid particles. If the particle size is assumed to be much larger than the thickness of the electrical double layer, i.e. $a\kappa \gg 1$, then the electrophoretic flow rate of solid material can be given by:

$$\frac{dV_{ep}}{dt} = \frac{\varepsilon_{rs}\varepsilon_0\zeta}{\mu} E_s(1-\phi_s)A \tag{2.52}$$

where V_{ep} is the volume of solid material transported by electrophoresis. For an electrofiltration experiment with the cathode placed beneath the filter medium the filter cake growth can then be determined by a mass balance of the solid material:

$$A\frac{dh}{dt}(\phi_c - \phi_s) = \left(\frac{dV_p}{dt} + \frac{dV_{eo}}{dt}\right)\phi_s + \frac{dV_{ep}}{dt} \tag{2.53}$$

The electrophoretic influence on the filter cake growth results in a suspension solidosity that is not constant during the filtration operation. If the solidosity in the suspension above the filter cake is assumed to be homogeneous, then the suspension solidosity can be described by:

$$\phi_s(t) = \frac{(V_p + V_{eo})\phi_{s,0} + V_{cell}\phi_{s,0} - Ah\phi_c}{V_{cell} - Ah} \tag{2.54}$$

where $\phi_{s,0}$ is the initial solidosity of the suspension and V_{cell} the volume of the filter cell.

The temperature increase in the filter cell as a result of ohmic heating was included in the electrofiltration model. The temperature in the filter cell was measured experimentally and was used to account for the temperature dependence of the water viscosity with Equation (2.55) (Fox *et al.*, 2004):

$$\mu = 2.414 \cdot 10^{-5} \cdot 10^{247.8/(T-140)} \tag{2.55}$$

where T is the temperature in Kelvin.

3. Experimental

3.1. Filtration equipment

3.1.1. Pressure filtration

Filtration experiments were performed using a bench-scale equipment designed for measuring local filtration properties (Johansson and Theliander, 2003). A constant filtration pressure was applied using a pneumatic pressure piston capable of delivering pressures up to 6 MPa. The location of the piston was measured by a position sensor (Temposonic EP-V-0200M-D06-1-V0) and the filtrate was collected and weighed.

The filtration cell is cylindrical, of diameter 60 mm and height 175 mm, with its lower section being composed of a 115 mm high Plexiglas cylinder. The bottom of the filter cell is a perforated plate that supports the filter medium. Eight water-filled capillary tubes of different heights are mounted from the bottom of the filtration cell to measure the local pressure in the filter cake being formed. These tubes are connected to pressure transducers (Kristal Instrumente AG). Each tube has an opening of diameter 0.6 mm perpendicular to the direction of flow; the openings are placed 0.5, 1, 2, 3, 5, 7, 9 and 12 mm from the bottom plate.

The local solidosity in the filter cell is measured through the attenuation of γ-radiation. The γ-attenuation can be evaluated for any selected 1 mm horizontal slice of the filtration using a ^{241}Am γ-source (10^9 Bq) along with a NaI(Tl) scintillation detector (Crismatec Scintibloc™, ORTEC DigiBASE) placed on a moveable rack. The number of observations was recorded in the energy range 33-83 keV for the microcrystalline cellulose studies and 36-91 keV for titanium dioxide. The local solidosity of the filter cake was calculated from the γ-attenuation measurements using the Beer-Lambert law for two phases, as given in Equation (3.1) (Bergström, 1992):

$$-ln\frac{n_\gamma}{n_{\gamma,0}} = \mu_{\gamma,l}d_\gamma + \left(\mu_{\gamma,s} - \mu_{\gamma,l}\right)d_\gamma\phi \tag{3.1}$$

where n_γ and $n_{\gamma,0}$ are the count number of radiation observations from the detector made during measurement and for the empty filtration cell, respectively. The average path length of the γ-radiation in the filter cell is denoted d_γ while $\mu_{\gamma,l}$ and $\mu_{\gamma,s}$ are the attenuation coefficients of the liquid and solid phases, respectively, in the energy range studied. The attenuation coefficients were determined through calibration with known filter cake solidosities:

attenuation coefficients of 19.7 m^{-1} for water, 29.1 m^{-1} for microcrystalline cellulose and 189 m^{-1} for titanium dioxide were obtained.

3.1.2. Electro-assisted filtration

The filtration equipment described in Section 3.1.1 was modified in order to study local filtration properties during electro-assisted filtration, see Figure 3.1. For the electro-assisted filtration experiments, the internal diameter of the filter cell was reduced to 50 mm for the 30 mm closest to the filter medium by means of a supporting rack.

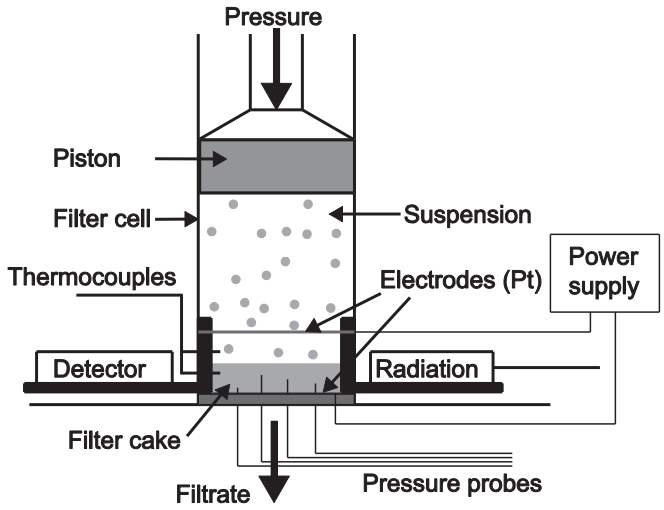

Figure 3.1. *Schematic diagram of the equipment used to study local filtration properties during the electro-assisted filtration experiments.*

The filter cell is equipped with two platinum electrodes connected to a DC power supply (EA-PSI 5299-02 A, Elektro-Automatik). An expanded platinum mesh (Unimesh 300) is placed beneath the filter medium and used as one of the electrodes. The other electrode is placed on a support rack inside the filter cell so that the electrodes are separated by a constant distance of 25 mm. In order to minimize interference with the suspension, this second electrode is a coarse mesh made of platinum wire, with a diameter of 0.127 mm, and has 10 mm square openings. For electro-assisted filtration of materials with a negative surface charge the cathode is placed beneath the filter medium. The voltage, current and power from the power supply is recorded during the experiments.

The local hydrostatic pressure within the filter cell is measured using four water-filled tubes, made of a non-conducting material (perfluoroalkoxy alkene, PFA), connected to pressure transducers. The tubes are mounted at the bottom of the filter cell and have openings with a diameter of 0.6 mm perpendicular to the direction of flow; the openings are placed 2, 4, 6 and 8 mm from the top of the filter medium. The temperature inside the filter cell is measured using two PFA coated K-type thermocouples located 5 and 20 mm from the filter medium, respectively.

3.2. Experimental procedure

3.2.1. Model materials

A commercially available microcrystalline cellulose (Avicel PH-105, FMC Biopolymers) was used to study the filtration behaviour of cellulosic particles. The material was subjected to mechanical treatment so that it could act as a model material for cellulosic materials with high specific surface areas. Additionally, a titanium dioxide (Acros organics) with an anatase content of at least 98 % (according to the product specifications) was used to study how agglomeration induced by an increasing ionic strength influences filtration behaviour.

3.2.2. Characterisation methods

The solid density of the microcrystalline cellulose was measured using a Micromeritics Accupyc II 1340. The particle size distribution was measured by laser diffraction using a Malvern Mastersizer 2000 with a detection range of 0.02-2000 μm (according to the equipment specifications). The pH dependence of the surface charge of the microcrystalline cellulose particles was determined through titration with a linear pDADMAC (polydiallyldimethylammonium chloride), using a Stabino 2.0 particle charge titration analyser (Particle Metrix GmbH).

The specific surface areas of the microcrystalline cellulose particles were measured by the BET method (8-point), using a Micromeritics Tristar 3000 with nitrogen as the adsorption gas. Cellulosic materials may experience pore collapse during drying from water, which lowers the specific surface area compared to the water-swollen state. The particles were therefore dried using a solvent exchange procedure (Haselton, 1955; Stone and Scallan, 1965), during which the water in the suspension was replaced sequentially by repeated displacement washing and resuspensions: first by acetone and then by cyclohexane (5 steps for each solvent). The particles were thereafter dried in a nitrogen stream at room temperature. The particles were also studied using a Zeiss Evo HD 15 scanning electron microscope.

In addition to the characterisation methods used for microcrystalline cellulose, the agglomeration behaviour of titanium dioxide was investigated at a suspension concentration of 1 % by volume using a Mettler-Toledo Focused Beam Reflectance Measurement (FBRM) G400 probe. The FBRM equipment measures the chord length distribution and has a detection range of 1-1000 μm (according to the equipment specifications). The ζ-potential of the titanium dioxide particles was determined using a Brookhaven Instruments ZetaPALS.

3.2.3. Suspension preparation

3.2.3.1. Modification of the particles' surface structure

The microcrystalline cellulose particles were suspended in deionised water to a solid content of 10 % by volume. The surface structure of the particles was modified through mechanical shearing using an IKA Ultra-Turrax® T50 with a S50N–G45F dispersing element submerged

in a baffled vessel with constant mixing conditions. Both the rotational speed of the dispersing element and the treatment time exerted a large influence on the effect of the mechanical treatment. The different treatments used in Articles I-IV were identified through characterisation of the material (as well as through filtration behaviour) to correspond to four different levels of mechanical treatment, see Table 3.1. Note that the rotational speed of the dispersing element affected the effectiveness of the mechanical treatment: a higher rotational speed required a lesser degree of treatment to obtain the same effect on the material being treated.

Table 3.1. *The mechanical treatments used on the microcrystalline cellulose suspensions, at a solid content of 10 % by volume, in Articles I-IV.*

	Article I	Article II	Article III	Article IV
Volume [dm^3]	5	5	4.5	4.5
Rotational speed [rpm]	7000	10 000	10 000	10 000
	Treatment [rev/g]	Treatment [rev/g]	Treatment [rev/g]	Treatment [rev/g]
No treatment	0	0	0	0
Treatment 1	269	-	-	-
Treatment 2	1077	269	269	269
Treatment 3	-	-	-	1186

3.2.3.2. Suspension conditions

After undergoing the mechanical treatment described in Section 3.2.3.1 the suspension conditions were adjusted for each condition investigated. In the studies of the local filtration properties of microcrystalline cellulose in Articles I and II, the filtration experiments were performed at the solid content of 10 % by volume. This was chosen so that thick filter cakes would be formed, thereby allowing measurements of the local filtration properties to be made over a wide range of solid compressible pressures during each filtration experiment. The suspensions were diluted to a solid content of 5 % by volume in the electro-assisted filtration experiments in Articles III and IV that focused on the dewatering rate.

The pH of the microcrystalline cellulose suspensions was 6.3. In filtration experiments performed at acidic conditions, it was adjusted to 2.9 by the addition of 1 M HCl and, for alkaline conditions, to 10.0 by the addition of 1 M NaOH. In the electro-assisted filtration experiments performed at different ionic strengths in Article IV, the ionic strength was adjusted through the addition of either 0.125 g $NaNO_3/dm^3$ or 0.5 g $NaNO_3/dm^3$.

In the electro-assisted filtration experiments performed on buffered suspensions in Article IV, 0.1 g Na_2CO_3/dm^3 was added. The pH of the suspension after this addition was 9.0; the buffered suspension had buffering ability to neutralise acidic electrolysis products.

The electrostatic interactions between the particles in the titanium dioxide suspensions studied in Article V were controlled by the ionic strength. The particles were suspended in deionised water; the pH of each suspension was 6.2. The ionic strength of the suspensions was adjusted

by the addition of sodium chloride. Suspensions with a low ionic strength (i.e. with no sodium chloride added) were compared with sodium chloride additions of 2 g/dm^3 and 10 g/dm^3.

The prepared suspensions were left in a mixing vessel at constant conditions for a minimum of 12 hours before the filtration experiments were initiated. The ambient temperature and starting temperature of the suspensions were constant, at about 23°C.

3.2.4. Filtration experiments and filter medium

The filtration behaviour of microcrystalline cellulose was studied using hydrophilic polyethersulphone filters (Pall Corporation, Supor®) with a nominal pore size of 0.45 μm (according to the product specification). Additional experiments were also performed using hydrophilic polyethersulphone filters (Pall Corporation, Supor®) with pore sizes of 0.1 and 0.8 μm to investigate possible blinding of the filter medium. The filtration properties of titanium dioxide suspensions were studied using regenerated cellulose membranes (Sartorius stedim, Type 184, nominal pore size 0.2 μm). All filtration experiments were performed using an additional Grade 5 Munktell filter to provide mechanical support.

Additional experiments were performed during studies of the electroosmotic dewatering of microcrystalline cellulose, without either the polyethersulphone filter or the support filter, in order to verify that the filter medium setup being employed had no significant influence on the dewatering rate or the electrical resistance of the system. The combined flow resistance of the filter medium and the support filter used in the experimental setup was measured as being $1.4 \cdot 10^{10}$ m^{-1} for water without cellulosic particles.

The pH profile in the filter cake during electrofiltration was measured by dissecting cakes from aborted filtration experiments. Each of these filter cakes was split into 4 equal segments before the pH was measured using pH indicator paper.

3.3. Material characterisation

3.3.1. Microcrystalline cellulose

3.3.1.1. Particle properties

The microcrystalline cellulose was characterised using the methods described in Section 3.2.2. When suspended in water, the microcrystalline cellulose particles are porous and water-swollen (Luukkonen *et al.*, 2001). Particles of the same grade and manufacturer as used in this study have been found to have a water content of 0.47 ± 0.02 g H_2O/g at a neutral pH (Köhnke *et al.*, 2011), a content that corresponds to a particle solidosity of 0.58. The solid density of the dry particles was measured as being 1560 kg/m^3. Figure 3.2 is an image of the dry microcrystalline cellulose particles obtained using SEM microscopy. Although the shapes of the particles vary significantly, they can best be described as being somewhat cylindrical. Their surfaces can be seen as being rather smooth, even if some fragmentation and pore openings can be detected.

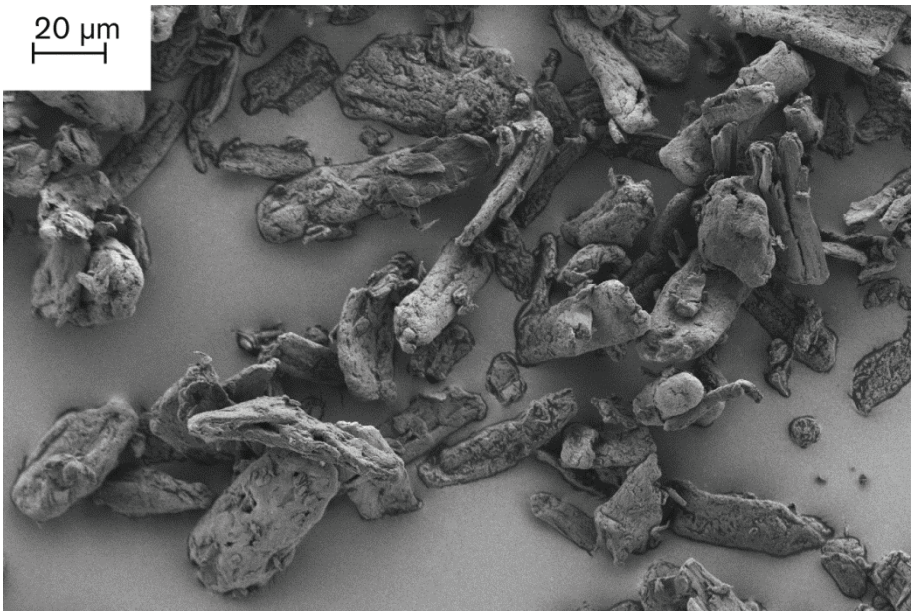

Figure 3.2. *SEM photograph of dry microcrystalline cellulose particles.*

The specific surface area of the microcrystalline cellulose particles as delivered from the manufacturer was measured using the BET technique and a value of 2.1 m^2/g was obtained. Although affected by irregularities in the shape, as well as some pores and cracks, of the particle this measurement is mainly attributed to the external surface of the particles. For filtration purposes, it is important to differentiate between the external and internal surface areas of particles because the contribution they make to the filtration behaviour differs. The total specific surface area measured using BET (including both the external and internal area) was 43 ± 1 m^2/g for the microcrystalline cellulose particles that were suspended in water and then dried after undergoing the solvent exchange procedure described in Section 3.2.2 to avoid closure of the pores and preserve the swollen structure of the particles.

The surface charge of the microcrystalline cellulose was measured by titration with a linear pDADMAC; the pH dependence is shown in Figure 3.3. The particles' surfaces are charged at neutral and alkaline conditions; at acidic conditions, the charge is close to zero due to the neutralisation of acidic groups (Araki *et al.*, 1999).

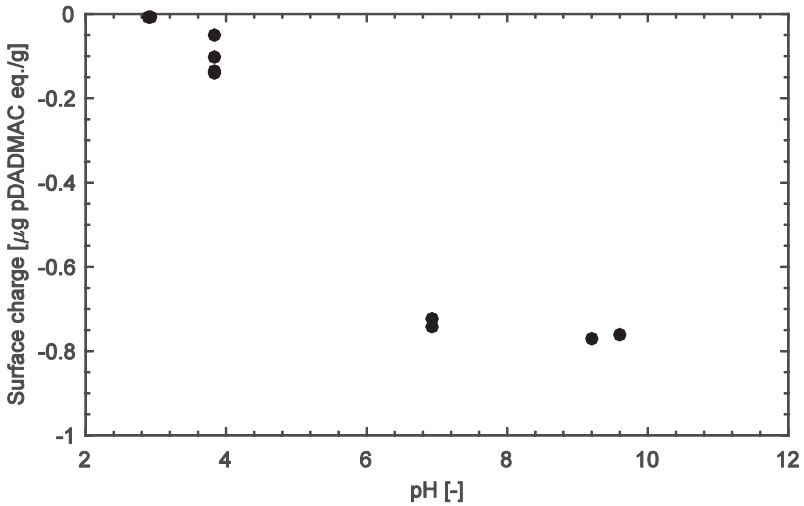

Figure 3.3. *The surface charge of microcrystalline cellulose particles measured by titration with a linear pDADMAC.*

3.3.1.2. Surface modification and specific surface area

The microcrystalline cellulose particles were subjected to different degrees of mechanical treatment in order to modify their surface structure and thereby the specific surface area of the material. The effect of this mechanical treatment is shown clearly in the SEM photographs presented in Figure 3.4. Figure 3.4a shows the surface of a microcrystalline cellulose particle not subjected to mechanical treatment: it is mostly smooth, with fragments of a few microns in size observable. The surface structures of microcrystalline cellulose particles subjected to the different degrees of mechanical treatment used in Article I are shown in Figure 3.4b and Figure 3.4c. The ruggedness of these surfaces increased as the particles were subjected to more mechanical treatment: at the greatest degree of mechanical treatment, Figure 4.3c, web-like fibrillation covered large sections of the surfaces.

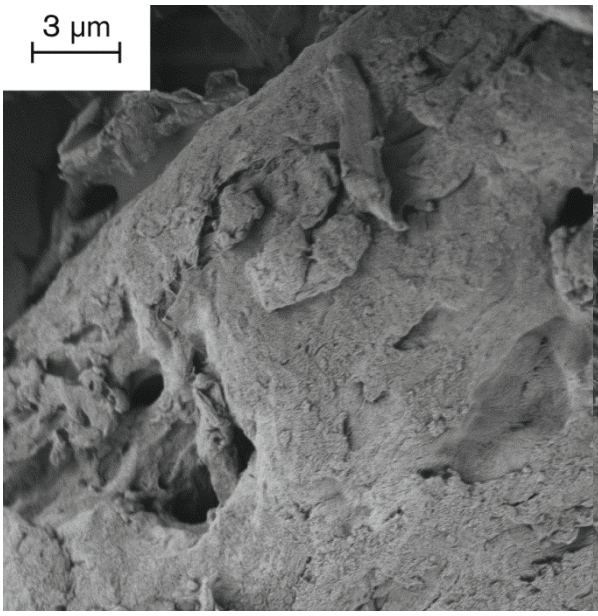

Figure 3.4a. *SEM photograph of the surface of a microcrystalline cellulose particle not subjected to mechanical treatment. The sample was dried after undergoing a solvent exchange procedure.*

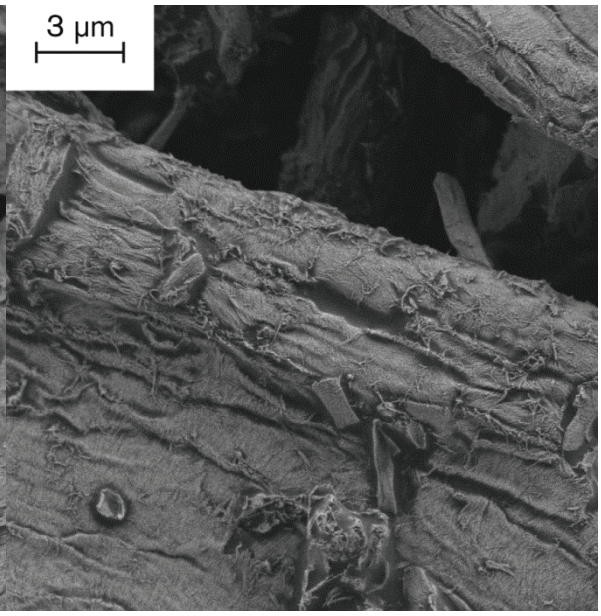

Figure 3.4b. *SEM photograph of microcrystalline cellulose subjected to the lower degree of mechanical treatment in Article I. The sample was dried after undergoing a solvent exchange procedure.*

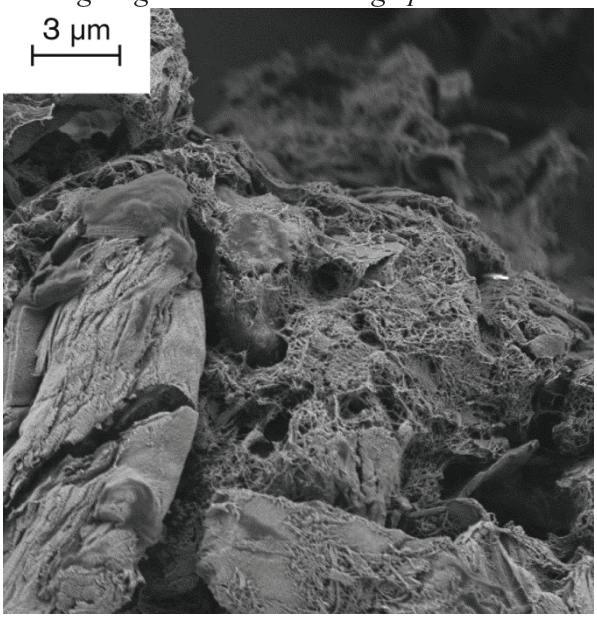

Figure 3.4c. *SEM photograph of microcrystalline cellulose subjected to the higher degree of mechanical treatment in Article I. The sample was dried after undergoing a solvent exchange procedure.*

Figure 3.4a-c show that mechanical treatment increases the surface ruggedness of microcrystalline cellulose particles; the effect was quantified using the BET technique which measured the specific surface areas. Suspensions subjected to the various degrees of mechanical treatment described in Section 3.2.3.1 were dried from cyclohexane after undergoing a solvent exchange procedure; the measured specific surface areas are presented in Table 3.2. If it is assumed that the increase in the specific surface area is solely an effect of increasing the external surface area of the particles, the specific external surface area at various degrees of mechanical treatment can then be estimated, see Table 3.2.

Table 3.2. *The effect of mechanical treatment on the specific surface area of the particles, measured by the BET technique and calculated from the particle size distribution measured by laser diffraction. An estimation of the external particle surface area, obtained from the BET measurements, is also included.*

Mechanical treatment[a]	A_{BET}[b] [m^2/g]	A_{ext}[c] [m^2/g]	A_{LD}[d] [m^2/g]
No treatment	43 ± 1	2 ± 1	0.40
Treatment 1	48 ± 3	7 ± 3	0.44
Treatment 2	50 ± 4	9 ± 4	0.49
Treatment 3	-	-	0.55

[a] Mechanical treatment reported in Table 3.1.
[b] BET specific surface area (95 % confidence interval) of particles dried using a solvent exchange procedure.
[c] Calculated from BET measurements under the assumption that the internal surface area is unaffected by the mechanical treatment.
[d] Calculated from laser diffraction measurements under the assumption that the particles are smooth spheres with a solidosity of 0.58.

The effect of the mechanical treatment to which the particles were subjected is not, however, isolated to their external surfaces. Figure 3.5 shows the particle size distribution of microcrystalline cellulose particles subjected to mechanical treatment. Increasing the degree of mechanical treatment resulted in a somewhat decrease in the particle size. The contribution made by particle breakage to the external surface area was estimated from laser diffraction measurements under the assumption that the particles are smooth, spherical and porous with a solidosity of 0.58; the results are reported in Table 3.2. The estimated effect of mechanical treatment on the specific surface area estimated from laser diffraction was found to be very small compared to that observed by BET measurements. This indicates that the effect of generating a greater surface area by breaking up particles is small compared to the effect of increasing the roughness of the surface. The increase observed in the specific surface area from BET measurements is thus mainly attributed to changes in the surface structure of the particles.

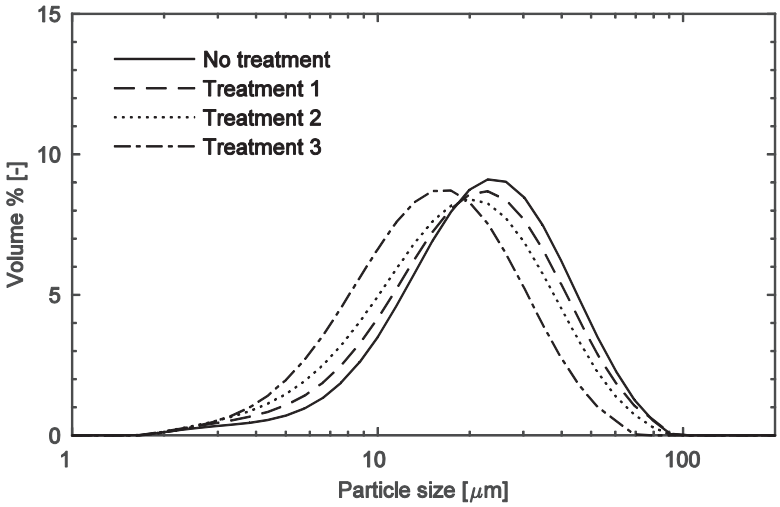

Figure 3.5. *Volume-based particle size distribution of microcrystalline cellulose subjected to varying degrees of mechanical treatment. The particle size distribution was measured by laser diffraction.*

3.3.2. Titanium dioxide

The titanium dioxide particles used in Article V had a solid density of 3810 kg/m^3. The specific surface area, determined from BET measurements, was 9.8 m^2/g and the ζ-potential of the particles suspended in deionised water, at a suspension pH of 6.2, was -22 ± 2 mV. Figure 3.6 shows a SEM photograph of a dry agglomerate of titanium dioxide particles.

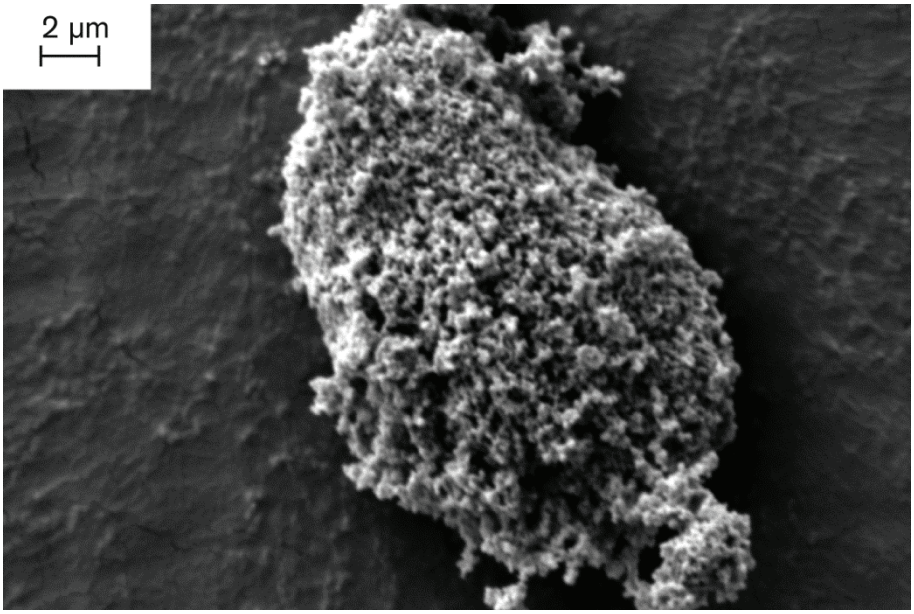

Figure 3.6. *SEM photograph of a dry agglomerate of titanium dioxide.*

The agglomeration behaviour of titanium dioxide particles was investigated by altering the ionic strength of the suspension. The particle size distribution measured at low concentrations using laser diffraction is shown in Figure 3.7. Two separate size ranges were observed at low ionic strengths, whereas only a narrow size distribution of agglomerates was obtained when the ionic

strength was increased. A small difference was observed between sodium chloride additions of 2 g/dm^3 and 10 g/dm^3: particles in the lower size range were still observed at additions of 2 g/dm^3. Nevertheless, both levels of ionic strength were found to mitigate the influence of the electrostatic interactions between the particles enough to allow extensive agglomeration to occur.

The chord length distribution was evaluated by focused beam reflectance measurement (FBRM) and is shown in Figure 3.8 for a suspension concentration of 1 % by volume. It was unaffected by sodium chloride additions of 1 g/dm^3 at the measurement conditions, although agglomeration was observed for sodium chloride additions of 2 g/dm^3. Addition of sodium chloride above 2 g/dm^3 was found to further increase the chord length distribution. This indicates that the electrostatic interactions have an effect on the stability of the agglomerates formed.

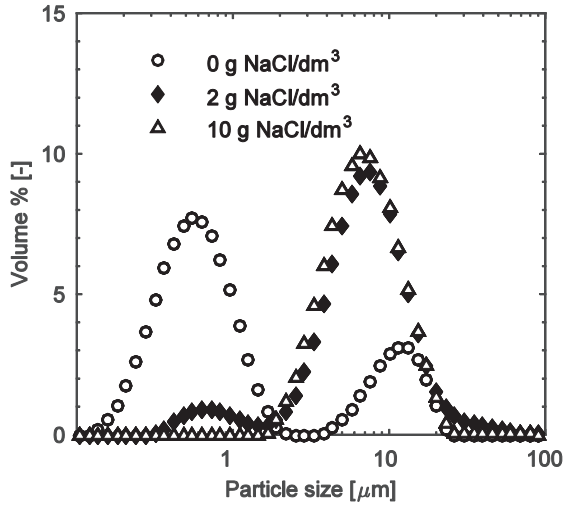

Figure 3.7. *Volume-based size distribution of titanium dioxide suspensions of varying ionic strengths, measured by laser diffraction.*

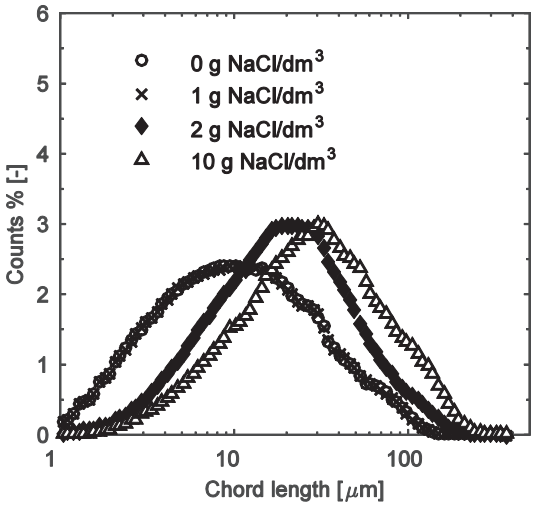

Figure 3.8. *Chord length distribution of titanium dioxide agglomerates at varying ionic strengths, measured by FBRM.*

4. Results and discussion

The filtration behaviour and electro-assisted dewatering of microcrystalline cellulose is discussed in Chapter 4. This chapter is divided into two subsections: Section 4.1 discusses the influence of particle properties and suspension conditions on the filtration behaviour and Section 4.2 the use of electroosmotic dewatering and electro-assisted filtration.

4.1. Filtration behaviour

4.1.1. Influence of the surface structure of particles

The effect of particle surface structure on the filtration behaviour of microcrystalline cellulose was studied for suspensions with an initial solids content of 10 % by volume and at a suspension pH of 2.9: this study is presented in Article I. The particle surface roughness was increased through mechanical shearing for characterisation of the particle surface, as described in Section 3.3.1.2. The influence of the particle surface structure on the filtrate volume obtained during filtration operations at a constant applied pressure is given in Figure 4.1. Increasing the surface roughness of the microcrystalline cellulose particles was found to decrease the filtrate flow rate to a large extent.

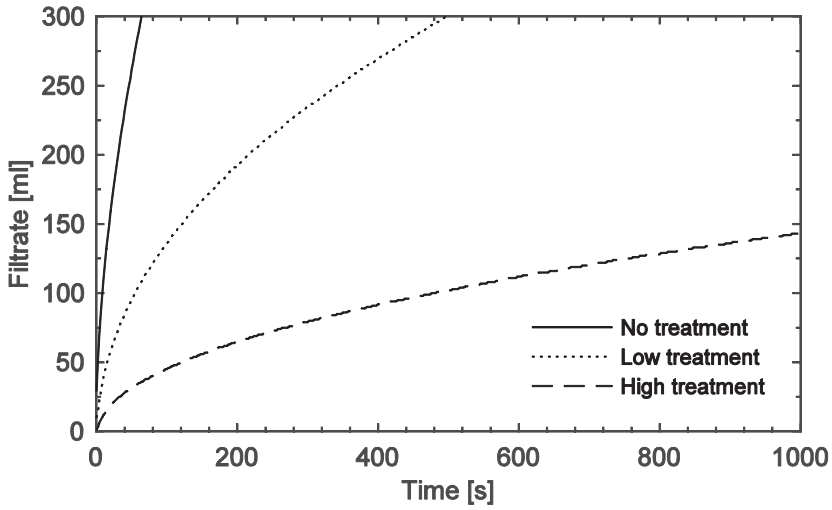

Figure 4.1. *The influence of the particle surface structure on the accumulated filtrate for filtration at an applied pressure of 0.3 MPa and a suspension pH of 2.9.*

The effect the mechanical treatment has on the local solidosity of the filter cake is shown in Figure 4.2 as a function of the local compressive pressure. During the filtration experiments no significant difference was observed between the two degrees of mechanical treatment. The similar solidosities of filter cakes at the various degrees of mechanical treatment thus indicate that the effect on the filtrate flow rate observed in Figure 4.1 is not primarily due to changes in the filter cake solidosity but is, instead, caused by the flow behaviour around individual particles. However, a difference in solidosity was observed during sedimentation experiments: no sedimentation was observed for the mechanically-treated systems at a suspension solidosity of 0.1 whereas the microcrystalline cellulose particles not subjected to mechanical treatment settled with an average sediment solidosity about 0.2. Mechanical treatment thus appears to increase the attractive particle interactions and results in an increasing network formation. As the local solidosity of the filter cake was unaffected by the degree of mechanical treatment in the pressure range investigated, the different network structures observed during the sedimentation experiments were compressed in the early stages of the formation of the filter cake.

The relationship between the local filter cake solidosity and the local specific filtration resistance is shown in Figure 4.3. The degree of mechanical treatment can be seen to have a large influence on the specific filtration resistance at the same filter cake solidosity. This effect can be described by the specific surface area: particles with an increased surface ruggedness have a larger external surface area that can be subjected to drag, thereby resulting in an increased specific filtration resistance.

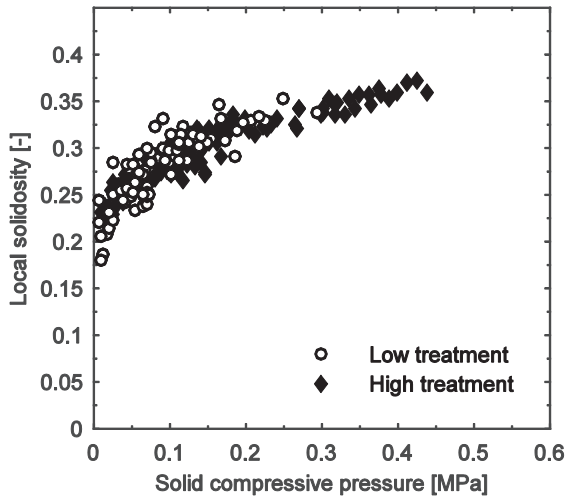

Figure 4.2. *The influence of the particle surface structure on the local filter cake solidosity at different degrees of mechanical treatment and a suspension pH of 2.9.*

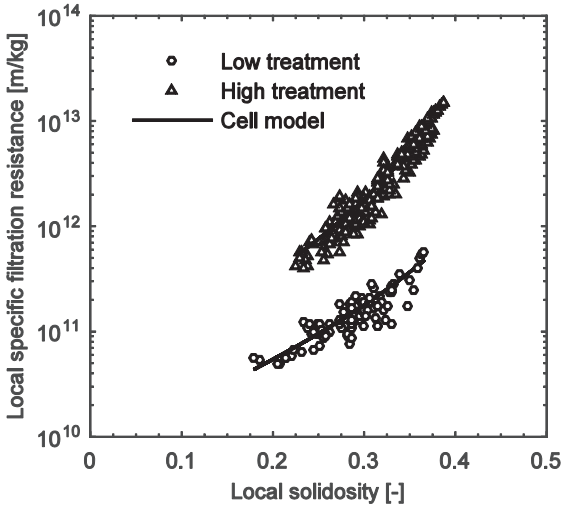

Figure 4.3. *The influence of the particle surface structure on the relation between the local filter cake solidosity and the local specific filtration resistance at a pH of 2.9.*

The cell model described in Section 2.2.1.2.2 is fitted to the experimental data and included in the figure.

As the surface structure of the microcrystalline cellulose particles is found to affect the specific filtration resistance without having a significant effect on the filter cake solidosity, modelling the effect on filtration behaviour is focused here on describing the relationship between these two filtration properties. This relationship can be described by the permeability relationships given in Section 2.2.1.2. The cell model shown in Figure 4.3, describing the system as flow around an impermeable porous sphere, was fitted to the experimental data and was able to accurately describe the relationship that had been determined experimentally. The two fitting parameters in the model, i.e. the radius and the solidosity of a spherical particle, are reported in Table 4.1 for the two degrees of mechanical treatment.

Table 4.1. *The parameters of the cell model in Section 2.2.1.2.2 fitted to the local filter cake solidosity and local specific filtration resistance at two degrees of mechanical treatment and a suspension pH of 2.9. The corresponding specific surface areas subjected to drag, and calculated from the parameters, are also included.*

Mechanical treatment	a [μm]	ϕ_i [-]	S_p [m^2/g]
Low	1.12	0.576	3.0
High	0.58	0.484	6.8

At the low degree of mechanical treatment, the radius of the sphere was the only model parameter used to fit the cell model to the experimental data; the solidosity of the sphere was taken as the particle solidosity estimated from measurements of the fibre saturation point (Köhnke *et al.*, 2011). At the high degree of mechanical treatment, on the other hand, both the sphere solidosity and the diameter of the sphere were used as model parameters. The cell model describes the microcrystalline cellulose particles as having a lower particle solidosity when the degree of mechanical treatment, and thus their surface roughness, is increased.

The cell model describes the microcrystalline cellulose particles as decreasing in size as the mechanical treatment is increased. The specific surface area subjected to drag is thus increased and results in a higher specific filtration resistance. However, the specific surface area subjected to drag is not only an effect of the size of a particle but also largely influenced by its surface structure. The relevant interpretation of the particle radius parameter in the model is therefore in terms of the effect the parameter has on the external specific surface area of the material. The fitted parameters from the cell model can be used to calculate the specific surface area subjected to drag, and the calculated values are included in Table 4.1. The specific surface areas of the model are in the same order of magnitude as the external specific surface area of the particles for both degrees of mechanical treatment; the external specific surface area is estimated from experimental measurement in Section 3.3.1.2 and reported in Table 3.2.

4.1.2. The influence of particle surface charge

4.1.2.1. Microcrystalline cellulose

The effect of the particle surface charge on the filtration behaviour of microcrystalline cellulose was studied using suspensions with an initial solids content of 10 % by volume, and is presented in Article II. The charge of the particle surfaces was modified through the pH of the suspension; the pH dependence of the particle surface charge is given in Figure 3.3 in Section 3.3.1.1. The influence of the particle surface charge on the filtration rate is given in Figure 4.4. The filtration rate is much lower at neutral conditions, when the particle surfaces are negatively charged, than at acidic conditions, where the particle surface charge is close to zero.

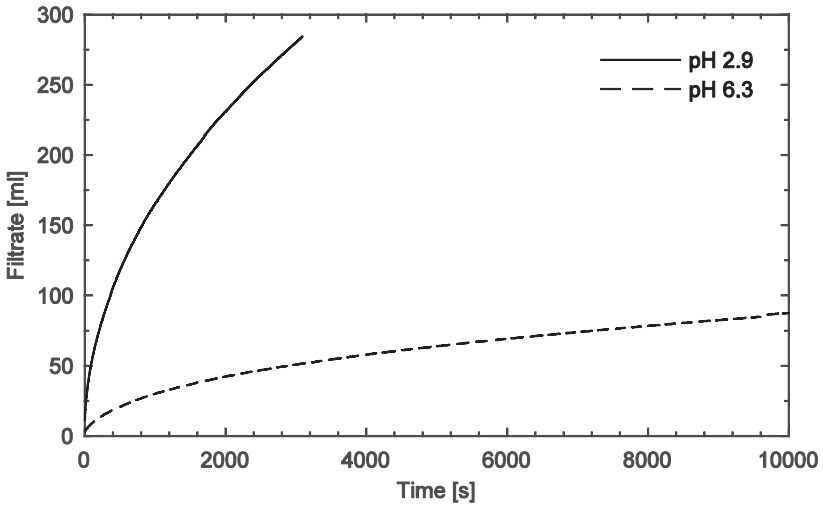

Figure 4.4. *The influence of particle surface charge on the accumulated filtrate for filtration at an applied pressure of 0.3 MPa.*

The influence of the particle surface charge on the pressure dependence of the local filter cake solidosity is given in Figure 4.5. The filter cake appears to have a somewhat lower solidosity at low compressive pressures for acidic suspensions, indicating that attractive particle interactions increase the stability of the filter cake formed. At neutral conditions, when the particle surfaces are charged, this stability is counteracted by electrostatic repulsion and the filter cake is more readily compressed. The pressure dependence of the filter cake solidosity was described by the constitutive relationship in Equation (2.11); the fitted model parameters for the two different pH levels are given in Table 4.2. The fitted relationship is included in Figure 4.5 and the relationship is extrapolated to a solid compressible pressure of 0.7 MPa (the maximum filtration pressure applied in Article II) in order to cover the entire range of compressive pressure in the filter cake.

Table 4.2. *The parameters of the solidosity relationship given in Equation (2.11) fitted to the filter cake solidosity measured in the experiments.*

Suspension pH	ϕ_0 [-]	P_a [Pa]	β [-]
2.9	0.2	9070	0.150
6.3	0.2	1520	0.108

The influence of the particle surface charge on the relationship between the specific filtration resistance and the filter cake solidosity is shown in Figure 4.6. At neutral conditions, when the particles surfaces are charged, the specific filtration resistance is an order of magnitude higher than for uncharged particles at the same filter cake solidosity. This behaviour is similar to the effect observed for particles with different surface structures discussed in Section 4.1.1. This effect may be explained by electrostatic repulsion from the charged surfaces of the particles, resulting in changes to the particle surfaces structure: close association between particles and particle fragments are prevented, thereby increasing the surface area in the filter cake that is subjected to drag forces from the passing fluid.

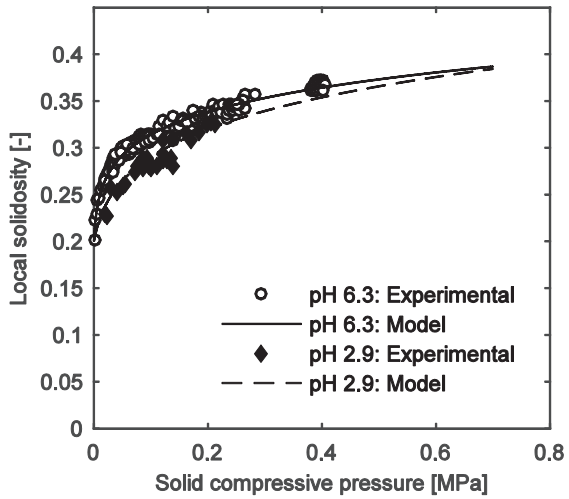

Figure 4.5. *Pressure dependence of the local filter cake solidosity for mechanically-treated microcrystalline cellulose suspensions at various pH levels.*

The constitutive relationship in Equation (2.11) is fitted to the experimental data and included in the figure.

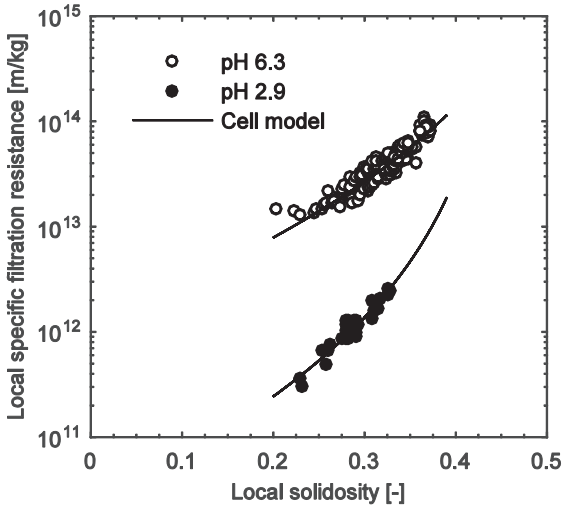

Figure 4.6. *Local specific filtration resistance as a function of local filter cake solidosity for mechanically-treated microcrystalline cellulose suspensions at various pH levels.*

The cell model described in Section 2.2.1.2.2 is fitted to the experimental data and included in the figure.

The relationship between the filter cake solidosity and the specific filtration resistance was described as flow around impermeable porous spheres according to the cell model given in Section 2.2.1.2.2. The cell model is included in Figure 4.6 and used to cover the entire solidosity range given by the solidosity relationship in Equation (2.11), at a maximum applied pressure of 0.7 MPa. The model parameters are given in Table 4.3 along with the corresponding specific surface area subjected to drag according to the cell model. The calculated specific surface area subjected to drag at acidic conditions is in the range of the external specific surface area of the microcrystalline cellulose particles that was estimated experimentally. At neutral conditions, on the other hand, the calculated specific surface area subjected to drag starts to approach the total specific surface area of the solid particles as measured by the BET technique, see Table 3.2 in Section 3.3.1.2. This behaviour may be interpreted as the charged particle surfaces increase the specific surface area as a result of electrostatic repulsion by particle fragments on the surface.

Table 4.3. *The parameters of the cell model described in Section 2.2.1.2.2 fitted to the local filter cake solidosity and local specific filtration resistance at different pH levels in the suspension. The corresponding specific surface areas subjected to drag, calculated from the parameters, are also included.*

Suspension pH	a [μm]	ϕ_i [-]	S_p [m^2/g]
2.9	0.769	0.465	5.38
6.3	0.095	0.566	35.7

4.1.2.2. Agglomerating systems

The influence of the particle surface charge on the filtration behaviour was also studied using titanium dioxide as a model material. The electrostatic particle interactions was modified through the ionic strength of the suspension; the results are presented in Article V.

The local solidosity of the titanium dioxide filter cakes is shown in Figure 4.7 as a function of the local compressive pressure. When the particles surfaces are charged, the titanium dioxide is found to form filter cakes of low compressibility. When the repulsive particle interactions are decreased by the addition of sodium chloride, however, the particles in the system agglomerate and form more compressible filer cakes of lower solidosity. The filter cake solidosity of the agglomerated systems remains lower than that of the non-agglomerated system throughout the filtration operation: agglomeration thus contributes to the formation of a porous network structure able to withstand significant compressive pressures.

The effect the ionic strength has on the relationship between the local solidosity and the local specific filtration resistance is shown in Figure 4.8 and was described as flow around impermeable solid spheres using the cell model given in Section 2.2.1.2.2. The model parameters, along with the corresponding specific surface areas, are reported in Table 4.4. In contrast to the behaviour of the microcrystalline cellulose discussed in Section 4.1.2.1, the main influence of the decreasing electrostatic particle interaction is through the change of the solidosity of the filter cake. The cell model does however describe the effect of agglomeration by decreasing the specific surface area subjected to drag somewhat. This implies that the effect of ionic strength observed on the local specific filtration resistance is not only an effect of the solidosity of the filter cake but also of changes to its structure that, in turn, shields the surface area from drag. This effect is, however, much more limited for the titanium dioxide than was observed for the microcrystalline cellulose in Section 4.1.2.1.

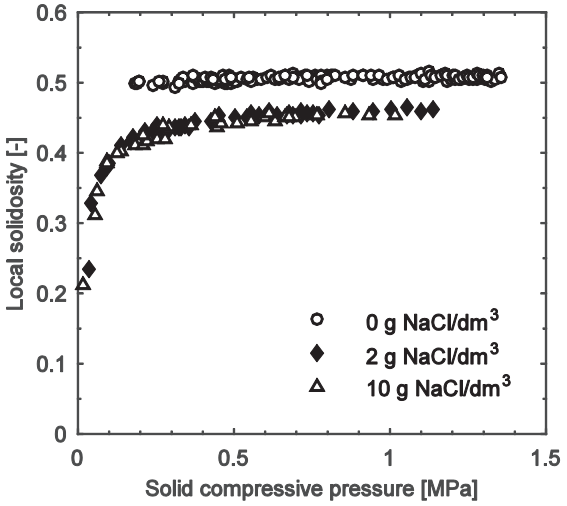

Figure 4.7. *Local solidosity as a function of the local solid pressure for titanium dioxide suspensions of different ionic strengths achieved by addition of sodium chloride.*

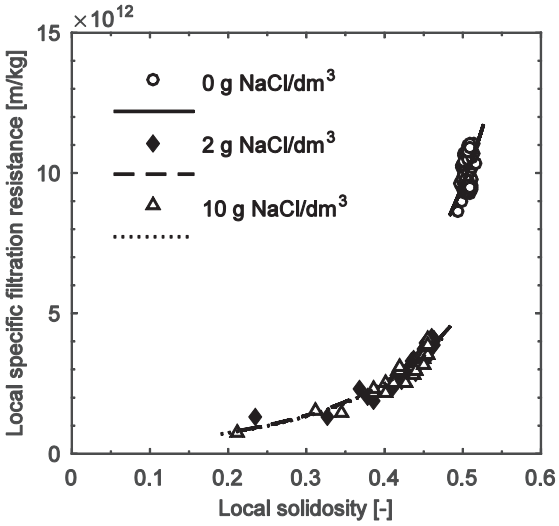

Figure 4.8. *Local specific filtration resistance as a function of local filter cake solidosity for titanium dioxide suspensions of different ionic strengths achieved by addition of sodium chloride. The cell model described in Section 2.2.1.2.2 is fitted to the experimental data and included in the figure as lines.*

Table 4.4. *Model parameter of the cell model described in Section 2.2.1.2.2 and the corresponding specific external surface areas for titanium dioxide suspensions at different ionic strengths.*

NaCl addition [g/dm^3]	a [μm]	S_p [m^2/g]
0	0.069	11.5
2	0.094	8.4
10	0.095	8.3

4.1.3. Modelling using local filtration properties

For filtration operations controlled by the flow resistance of the filter cake, the local filtration properties can be used to model the system using the approach described in Section 2.3.2. The use of experimental measurements of the local filtration properties means that a small number of filtration experiments, in theory even a single experiment, is sufficient to describe accurately, and even predict, the filtration behaviour at various applied filtration pressures and original solid contents of the suspension. The pressure dependence of the filter cake solidosity is described by an empirical relationship, Equation (2.11), and the relationship between the filter cake solidosity and the specific filtration resistance as flow around an impermeable porous sphere by the cell model given in Section 2.2.1.2.2.

The performance of the filtration model for microcrystalline cellulose in suspensions with different pH levels is evaluated using the model parameters given in Section 4.1.2. The

accumulated filtrate volumes taken from the model at two different applied filtration pressures are compared with experimental measurements at a suspension pH of 2.9 in Figure 4.9 and 6.3 in Figure 4.10. The filtration model is able to describe the experimental data accurately for both of the suspension conditions. The filtration model does not only give the filtrate flow rate but also describes the local properties of the filter cake. The modelled local hydrostatic pressure in the filter cake is compared with experimental measurements at different distances from the top of the filter medium throughout the filtration operation in Figure 4.11 and Figure 4.12 for suspensions with pH levels of 2.9 and 6.3, respectively. The modelled pressure profiles describe the experimental measurements accurately.

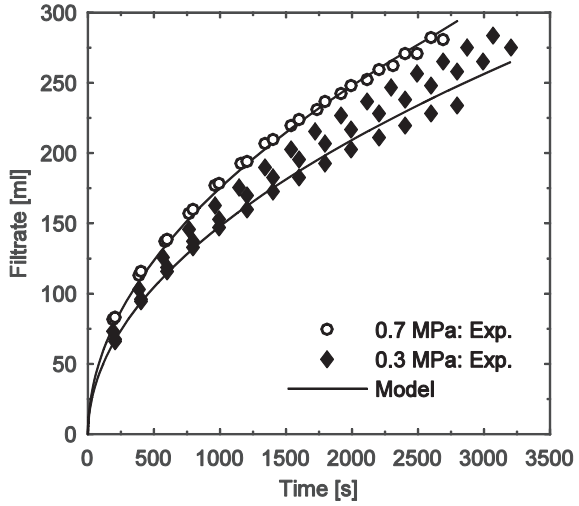

Figure 4.9. *Comparison of the modelled filtrate volume and the experimental measurements for mechanically-treated microcrystalline cellulose with a suspension pH of 2.9.*

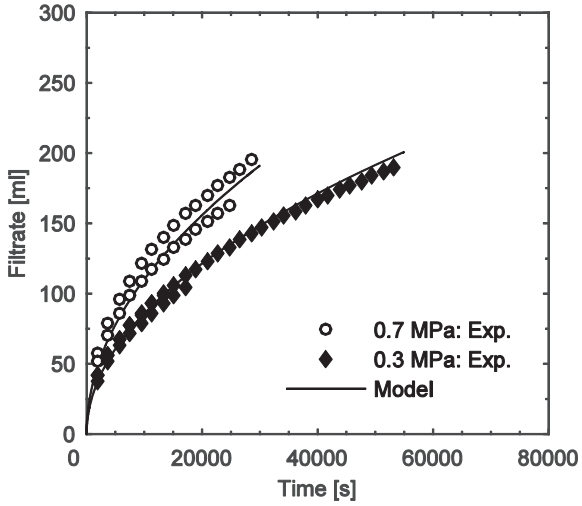

Figure 4.10. *Comparison of the modelled filtrate volume and the experimental measurements for mechanically-treated microcrystalline cellulose with a suspension pH of 6.3.*

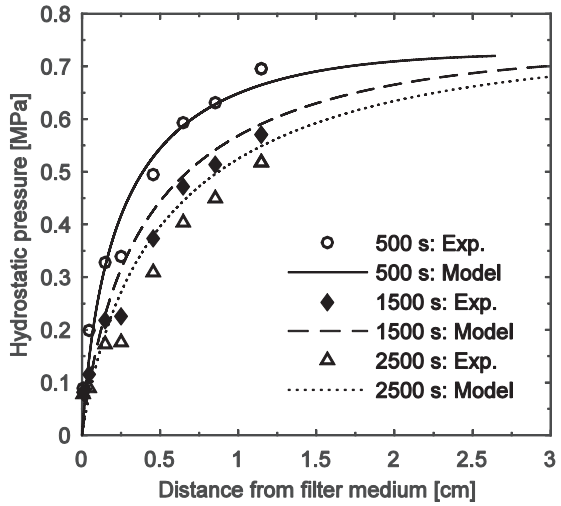

Figure 4.11. *Comparison of the modelled local hydrostatic pressure profile and the repeated experimental measurements for mechanically-treated microcrystalline cellulose at pH 2.9 and an applied pressure of 0.7 MPa.*

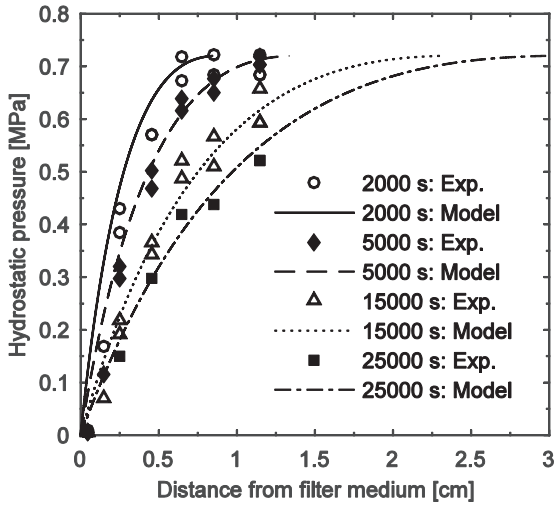

Figure 4.12. *Comparison of the modelled local hydrostatic pressure profile and the repeated experimental measurements for mechanically-treated microcrystalline cellulose at pH 6.3 and an applied pressure of 0.7 MPa.*

4.1.4. Summary of pressure filtration results

Increasing the surface roughness of microcrystalline cellulose particles resulted in a higher specific filtration resistance without influencing the filter cake solidosity in any major way. The relationship between the filter cake solidosity and the specific filtration resistance could be described by a cell model as flow around porous impermeable spheres.

The filtration resistance of microcrystalline cellulose suspensions is much higher at neutral or alkaline conditions, when the particles surfaces are charged, than at acidic conditions that give a low particle surface charge. The effect is more a result of charged particle surfaces increasing the specific surface area subjected to drag rather than of changes being made to the filter cake solidosity. This behaviour differs from the effect of particle surface charge on the filtration behaviour of an inorganic material such as titanium dioxide: for this type of material, the main effect of the surface charge is its influence on the filter cake solidosity through agglomeration.

Dead-end filtration operations dominated by the filtration resistance of the filter cake can be described accurately by a filtration model based on experimental measurements of the local filtration properties. Using experimental measurements of the local filtration properties allows the pressure dependence of a filtration operation to be determined from a small number of experiments.

4.2. Electro-assisted dewatering

The potential electro-assisted filtration has of facilitating the filtration of microcrystalline cellulose is illustrated in Figure 4.13 by applying an electric field midway through a pressure filtration operation. When the electric field is applied, a large increase in the filtrate flow rate is observed almost instantaneously. Similarly, Figure 4.14 shows that when an electric field is applied from the start of the filtration operation and removed midway through it, a rapid response in the filtrate flow rate can also be observed. This behaviour shows that an electric field has a potentially large influence on the dewatering of cellulosic materials.

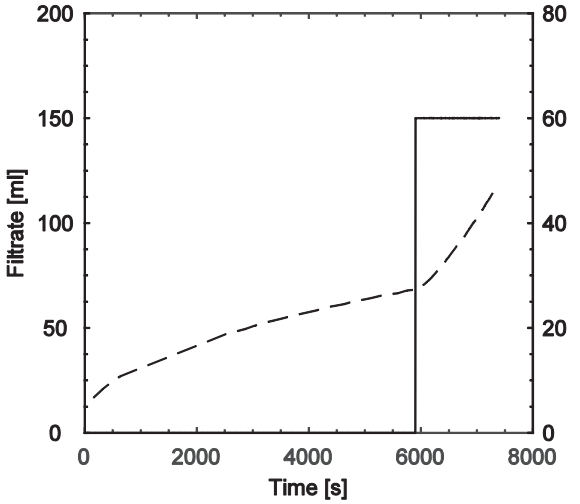

Figure 4.13. *Filtrate volume and applied voltage during the electrofiltration of a mechanically-treated microcrystalline cellulose.*

The suspension had a solid content of 5 % by volume and a starting pH of 6.3. The filtration pressure applied was 0.32 MPa.

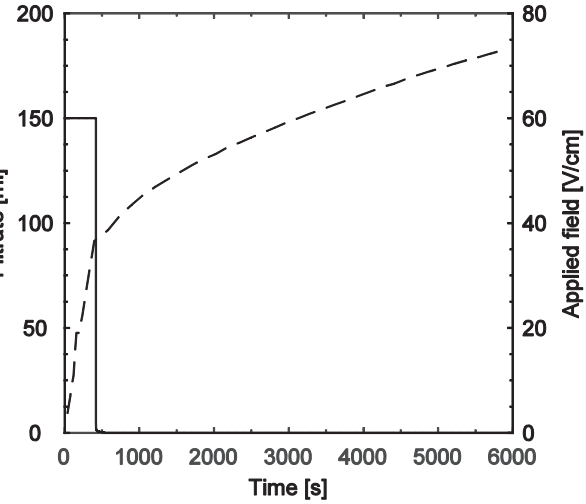

Figure 4.14. *Filtrate volume and applied voltage during the electrofiltration of a mechanically-treated microcrystalline cellulose.*

The suspension had a solid content of 5 % by volume and a starting pH of 6.3. The filtration pressure applied was 0.32 MPa.

In the following sections, the electrofiltration of microcrystalline cellulose suspensions with an initial solids content of 5 % by volume is discussed. The effect of electroosmosis is isolated, through the study of electroosmotic dewatering without an applied filtration pressure, in Section 4.2.1. The combined effects of electroosmosis, electrophoresis, ohmic heating and electrolysis reactions during electrofiltration are then discussed in Section 4.2.2, along with the influence of the specific surface area of the solid material and the ionic strength of the suspension. The contributions made by electroosmosis and electrophoresis to the electrofiltration behaviour are described by an electrofiltration model in Section 4.2.3 for a system at a low ionic strength in which the contributions from ohmic heating and electrolysis reactions are limited.

4.2.1. Electroosmotic dewatering

4.2.1.1. Electroosmotic flow rate

The filtrate volume obtained during the electroosmotic dewatering of microcrystalline cellulose without an applied filtration pressure can be seen in Figure 4.15: suspensions with two different levels of ionic strength and two different levels of constant applied voltage are shown. The electroosmotic flow rate was found to increase with the strength of the electric field. The electroosmotic dewatering rate of suspensions with an addition of 0.125 g $NaNO_3/dm^3$ was higher during the early stage of the dewatering operation compared to experiments performed at lower ionic strengths. This is contrary to the behaviour expected from the Helmholtz-Smoluchowski equation, Equation (2.35): increasing the ionic strength is expected to decrease the absolute value of the zeta-potential and thereby decrease the electroosmotic flow rate. A plausible explanation for the increase observed is that the surface conduction contributes to decreasing the electroosmotic flow rate at the lower ionic strengths. This behaviour is in agreement with previous studies that used bentonite and sodium kaolinite: the rate of electroosmotic dewatering increased as the ionic strength increased for salt concentrations of 10^{-3} to 10^{-2} M, which correspond to the salt additions used in this study (Ju *et al.*, 1991; Lockhart, 1983b). The electroosmotic flow rate may therefore be better described by a model that accounts for surface conduction.

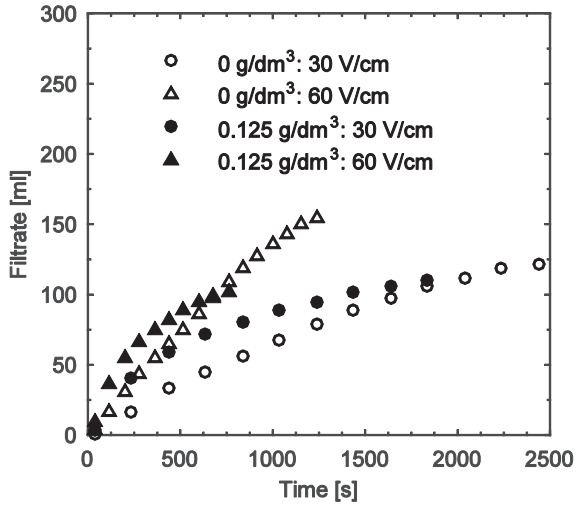

Figure 4.15. *Obtained filtrate during electroosmotic dewatering of microcrystalline cellulose suspensions at different ionic strengths achieved by the addition of $NaNO_3$.*

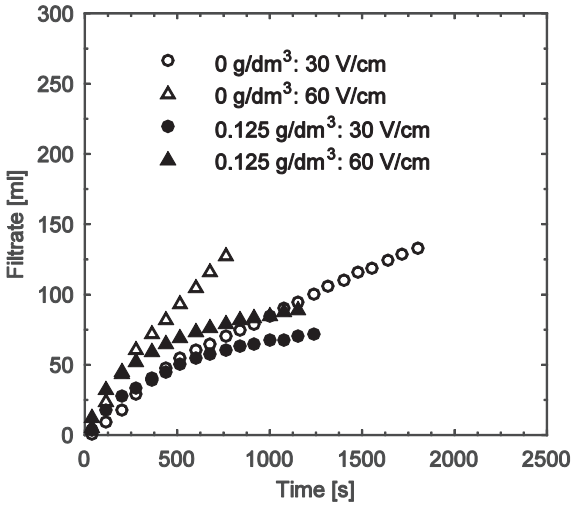

Figure 4.16. *Obtained filtrate during electroosmotic dewatering of a microcrystalline cellulose suspensions at the higher degree of mechanical treatment.*

The behaviour of a microcrystalline cellulose with a higher specific surface area during electroosmotic dewatering is given in Figure 4.16: it is similar to that observed of the microcrystalline cellulose of lower specific surface area given in Figure 4.15. The electroosmotic flow rate is thus found not to be largely decreased by the change in the specific surface area of the microcrystalline cellulose particles. This indicates that the specific surface

area of the microcrystalline cellulose particles does not increase the surface conductivity of the material in such a manner that it decreases the electroosmotic flow rate.

4.2.1.2. Electrolysis reactions

Figure 4.15 and Figure 4.16 show that the dewatering rate decreases during the electroosmotic dewatering operation. This effect is most pronounced at an increased ionic strength and at high applied voltages. Figure 4.17 shows the filtrate flow rate during electroosmotic dewatering at the applied voltage of 60 V/cm, and includes a suspension in which the ionic strength has been increased through the addition of $NaNO_3$ as well as a suspension to which Na_2CO_3 has been added to provide buffering ability. The buffered suspension neutralises the acidic electrolysis products at the anode. The filtrate flow rate of the buffered suspension does not decrease during the filtration operation in the same way as the suspension with $NaNO_3$ added to a similar ionic strength. The dewatering also continues further than for the suspension at a low ionic strength, without the addition of either salt, before the filtrate flow rate starts to decrease. This behaviour indicates that the decreasing rate of electroosmotic dewatering during the experiments is an effect of the electrolysis reactions lowering the pH in the filter cell, thereby decreasing the charge of the microcrystalline cellulose particles and, consequently, the electroosmotic flow rate.

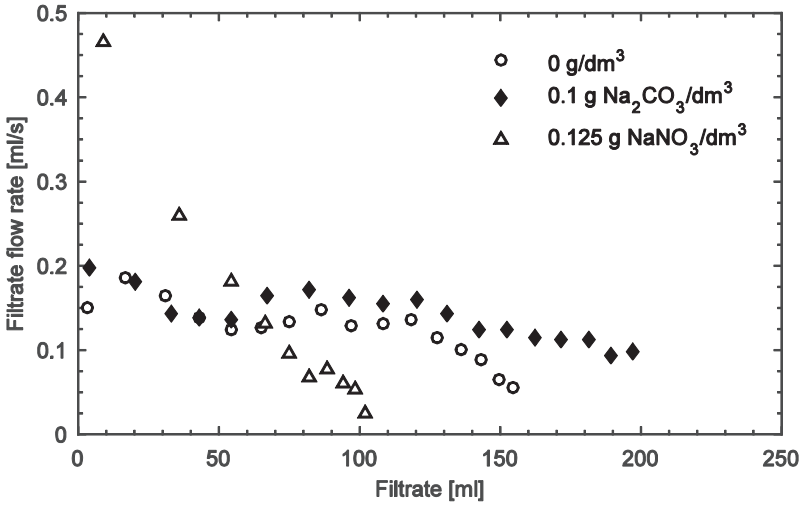

Figure 4.17. *Electroosmotic dewatering rate at an applied electric field of 60 V/cm for microcrystalline cellulose suspensions at varying ionic strengths, and for a suspension buffered with the addition of Na_2CO_3.*

4.2.1.3. Power demand

The power demand during electroosmotic dewatering is shown in Figure 4.18 for two levels of ionic strength. It increases during the early stages of the filtration operation: a result of a decreasing electrical resistance in the filter cell as ionic electrolysis products accumulate in the filter cell. It decreases, however, later on in the filtration operation. The decreasing power demand coincides with the decreasing rate of dewatering observed in Figure 4.17, and was not observed for the buffered suspensions. The effect is most pronounced at the increased ionic strength, when the current intensity is high and the electrolysis reactions are most prominent. This behaviour is similar to the increasing electrical resistance that can be observed during desiccation of filter cakes (Citeau *et al.*, 2016). The decreasing power demand was not observed during the electrofiltration experiments with an applied filtration pressure of 0.3 MPa, where the applied mechanical pressure limited the decrease in the filtrate flow rate, see Figure 4.29.

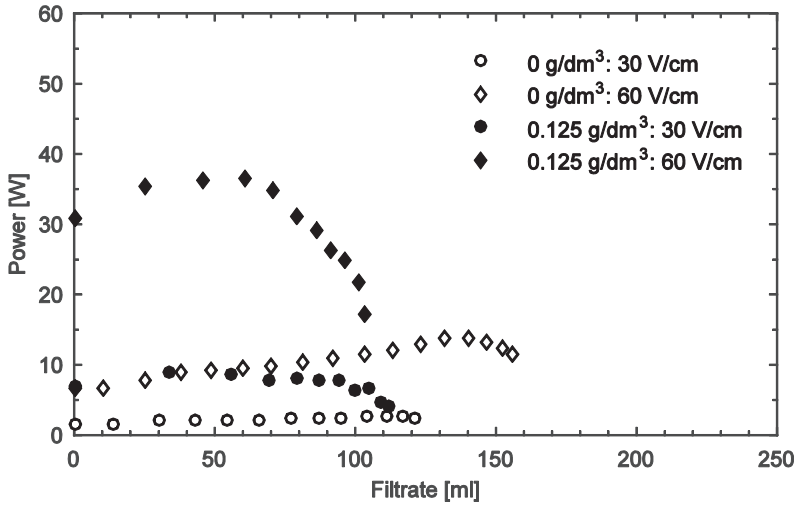

Figure 4.18. *Power demand during the electroosmotic dewatering of microcrystalline cellulose suspensions at varying additions of $NaNO_3$ and electric field strengths.*

4.2.2. Electrofiltration

The electrofiltration behaviour of a mechanically-treated microcrystalline cellulose was studied for suspensions with an initial solids content of 5 % and a low ionic strength. The filtrate volume obtained during the electrofiltration experiments at constant applied voltages are shown in Figure 4.19. The filtrate flow rate can be seen to increase with the strength of the electric field: the behaviour is similar to that of the electroosmotic dewatering in Figure 4.15. In addition to electroosmotic dewatering, an electrophoretic force will also act on the solid material in the opposite direction and influence the filter cake formation, thereby further influencing the filtrate flow rate during electro-assisted filtration.

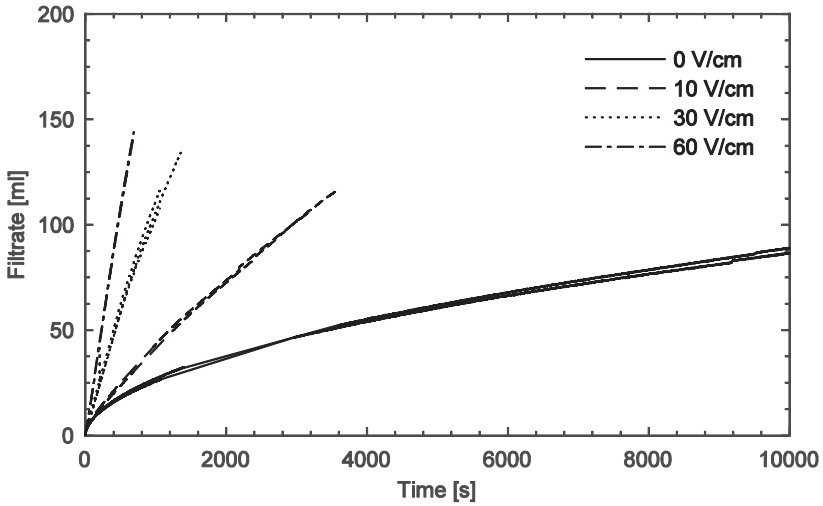

Figure 4.19. *Amount of filtrate accumulated during the electrofiltration of microcrystalline cellulose at pH 6.3 and various voltages at an applied filtration pressure of 0.32 MPa.*

The influence of the applied electric field on the formation of the filter cake can be observed through measurement of the local properties in the filter cell. The local hydrostatic pressure at different distances from the filter medium cell is given for pressure filtration without an applied electric field in Figure 4.20. The formation of a compressible filter cake results in a large fraction of the pressure drop being located close to the filter medium: as the filtration operation progresses and the filter cake grows, a pressure drop can be measured at a distance from the filter medium. The local hydrostatic pressure at an applied voltage of 10 V/cm is shown in *Figure* 4.21. No pressure drop can be measured by the pressure probes in the filter cell in the electro-assisted filtration experiments: a rate-limiting filter cake has therefore not been formed and the filtration rate is limited by the region close to the filter medium.

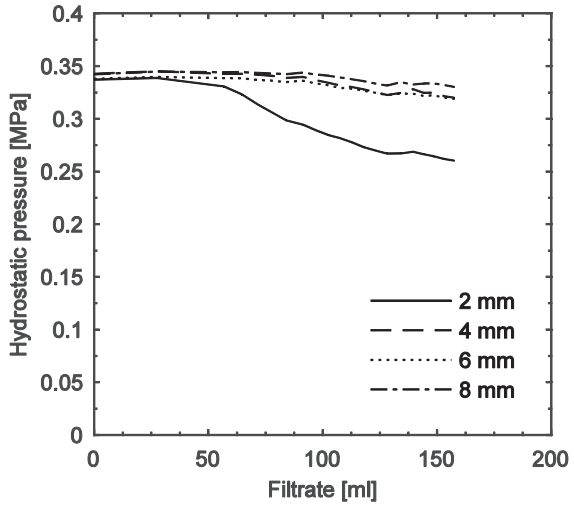

Figure 4.20. *Local hydrostatic pressure during the filtration of a microcrystalline cellulose suspension at pH 6.3 and a filtration pressure of 0.32 MPa.*

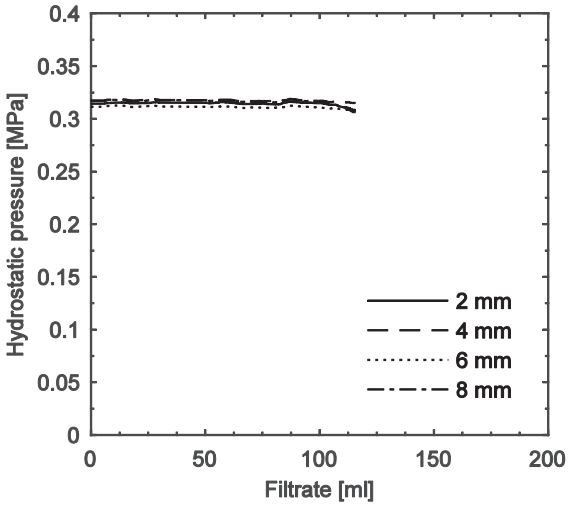

Figure 4.21. *Local hydrostatic pressure during the electrofiltration of a microcrystalline cellulose suspension at pH 6.3 and a filtration pressure of 0.32 MPa. Voltage applied: 10 V/cm.*

The influence of the electric field on the growth of the filter cake can be seen in Figure 4.22, where measurements of the filter cake's local solidosity made 6 mm from the filter medium are shown. In the filtration experiments without an electric field, the solidosity increased during the filtration operation: a result of the filter cake's growth as well as sedimentation in the filter cell. When an electric field is applied, the solidosity did not increase to the same extent. When voltages of 30 V/cm and 60 V/cm were applied, the measured solidosity corresponded to a thickening in the filter cell rather than growth of the filter cake or sedimentation. At an applied electric field of 10 V/cm the measured solidosity was found to be in between that of filter cake formation without an electric field and the thickening observed when electric fields of higher strengths were applied.

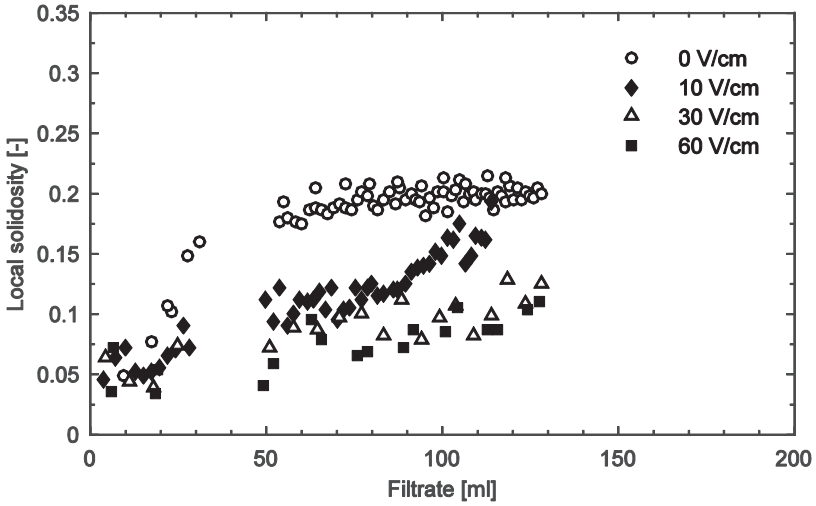

Figure 4.22. *Local solidosity measured 6 mm from the filter medium during filtration experiments at various applied voltages and a filtration pressure of 0.32 MPa.*

4.2.2.1. Influence of specific surface area

The pressure filtration behaviour, as discussed in Section 4.1.1, is greatly influenced by the specific surface area of the solid particles. The electroosmotic dewatering rate (discussed in Section 4.2.1.1), on the other hand, was found to be largely unaffected by the mechanical treatment of the microcrystalline cellulose particles. The influence of the specific surface area of microcrystalline cellulose particles on the electrofiltration behaviour is shown in in Figure 4.23 and Figure 4.24 by comparing the accumulated filtrate for two different degrees of mechanical treatment. The electro-assisted filtration rate is similar for the two systems, whereas the pressure filtration is largely dependent on the degree of mechanical treatment. The improvement of the dewatering rate obtained by electro-assisted filtration thus increases with the specific surface area of the solid material.

In Section 4.1.2 it was established that the specific filtration resistance of microcrystalline cellulose was largely influenced by the pH of the suspension: at acidic conditions, the filtration resistance was much lower than for neutral, or alkaline, conditions, where the particle surfaces are charged. The results of the pressure filtration of microcrystalline cellulose at a pH of 2.9 for the two degrees of mechanical treatment are included in Figure 4.23 and Figure 4.24. It can be

seen that the application of an electric field can have a greater influence on the dewatering rate than what could be achieved through modification of the suspension pH only: the difference becomes increasingly pronounced as the specific surface area of the material increases.

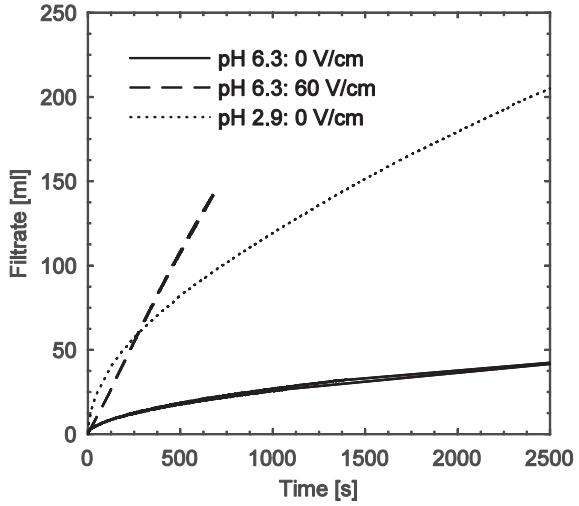

Figure 4.23. *Filtrate obtained during electrofiltration of microcrystalline cellulose suspensions at the lower degree of mechanical treatment using a filtration pressure of 0.3 MPa.*

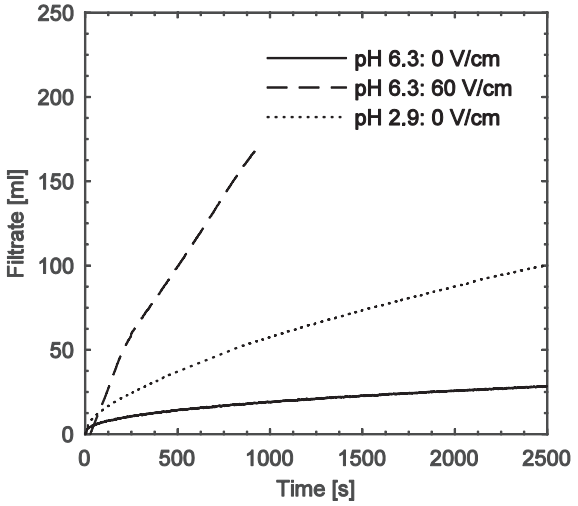

Figure 4.24. *Filtrate obtained during electrofiltration of microcrystalline cellulose suspensions at the higher degree of mechanical treatment using a filtration pressure of 0.3 MPa.*

4.2.2.2. Influence of ionic strength

The influence of ionic strength on the behaviour of electro-assisted filtration was studied using mechanically-treated microcrystalline cellulose suspensions with a solid content of 5 % by volume. The ionic strength of the suspensions was modified through the addition of $NaNO_3$ or, in the case of buffered suspensions, with the addition of Na_2CO_3.

The influence of ionic strength on the filtration behaviour of microcrystalline cellulose is given in Figure 4.25. The filtration resistance decreases, to a large extent, as the ionic strength of the suspension increases: this is an effect of the decreasing electrostatic repulsion between the particles and fragments thereof, as the increasing electrolyte content shields the surface charge of the particles. This is similar to the effect observed when the surface charge was modified by adjusting the pH of the suspension, as discussed in Section 4.1.2. Increasing the ionic strength of the suspension will thus not only influence the electrokinetic effects during electro-assisted filtration but also have a large influence on the behaviour of pressure filtration.

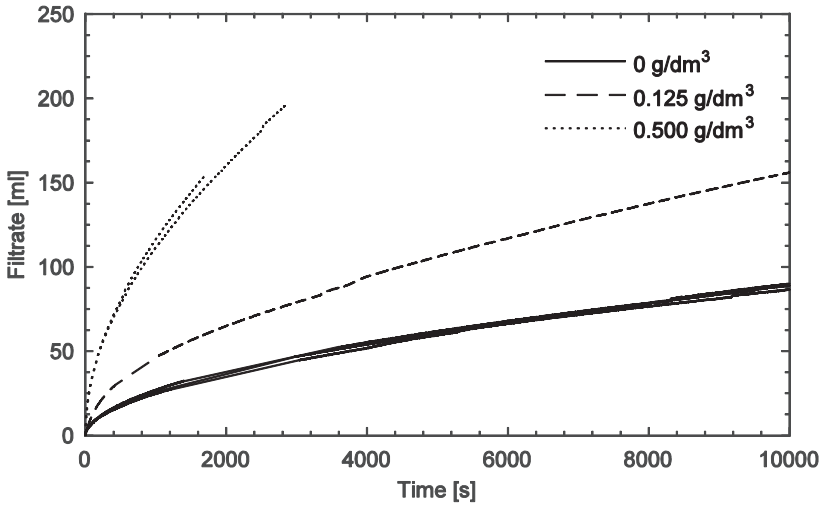

Figure 4.25. *Filtrate obtained from suspensions with different ionic strengths, achieved by the addition of $NaNO_3$, using a filtration pressure of 0.3 MPa and a suspension pH of 6.3.*

The filtrate volumes obtained during electrofiltration at various applied voltages are shown in Figure 4.26 and Figure 4.27 for microcrystalline cellulose suspensions of two different levels of ionic strength. The filtration rate can be seen to increase with the strength of the electric field for both ionic strengths. The maximum electric field applied in Figure 4.27 was limited to 30 V/cm due to the high power demand involved, see Section 4.2.2.3. Pressure filtration at a pH of 2.9, without the application of an electric field, is also included in Figure 4.26 and Figure 4.27. The filtrate flow rate obtained during electrofiltration can be seen to be lower than that obtained by lowering the pH of the systems. This behaviour implies that the specific filtration resistances of the microcrystalline cellulose in Figure 4.26 and Figure 4.27 are sufficiently low that the filtration pressure contributes considerably to the filtration operation, and also that electrokinetic action does not dominate the operation at these suspension conditions.

The pH in the filter cakes during the electro-assisted filtration experiments in Figure 4.26 and Figure 4.27 decreased as filtration progressed due to the electrolysis reactions at the anode. The pH profile was measured through dissection of filter cakes collected at various stages of the filtration operation. The pH in the filter cakes decreased in the direction of the anode (further away from the filter medium), becoming increasingly acidic during the filtration operation. The effect was more pronounced for systems with high ionic strengths and at high applied voltages. Decreasing the pH in the filter cell has a diminishing effect on the electroosmotic flow rate, as was discussed for the electroosmotic dewatering experiments in Section 4.2.1.

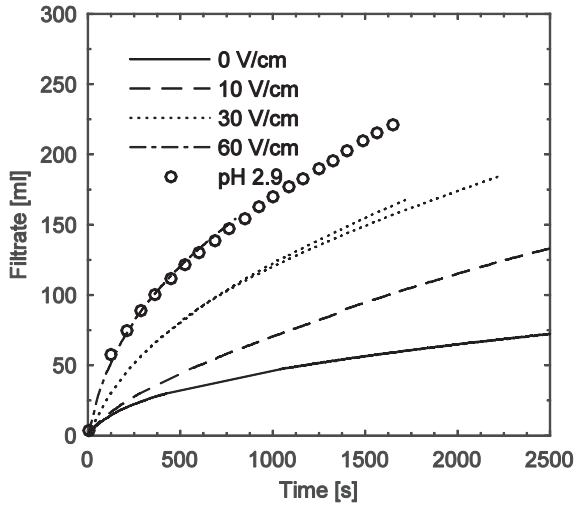

Figure 4.26. *Filtrate obtained during the electrofiltration of a mechanically-treated microcrystalline suspension with an addition of 0.125 g $NaNO_3/dm^3$ and a filtration pressure of 0.3 MPa. Pressure filtration at pH 2.9 without an electric field applied is included for reference.*

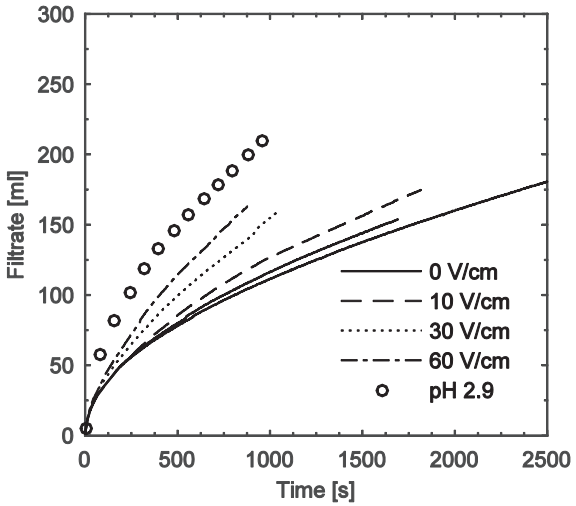

Figure 4.27. *Filtrate obtained during the electrofiltration of a mechanically-treated microcrystalline suspension with an addition of 0.5 g $NaNO_3/dm^3$ and a filtration pressure of 0.3 MPa. Pressure filtration at pH 2.9 without an electric field applied is included for reference.*

The effect of electrolysis reactions on the electrofiltration behaviour was counteracted by performing filtration experiments on buffered suspensions. The filtrate volumes obtained during electrofiltration of a buffered suspension, which neutralises the acidic electrolysis products, are given in Figure 4.28. During electrofiltration operations, the flow rate of the filtrate in buffered suspensions does not decrease to the same extent as in non-buffered systems of similar ionic strength: the flow rate is, instead, more or less constant throughout the whole filtration operation. This behaviour is similar to that observed in the electroosmotic dewatering experiments shown in Figure 4.17. The formation of acidic electrolysis products at the anode thus had a detrimental effect on the electro-assisted filtration of microcrystalline cellulose, highlighting the importance of preventing the electrolysis products from decreasing the surface charge of the solid material during the electrofiltration operation.

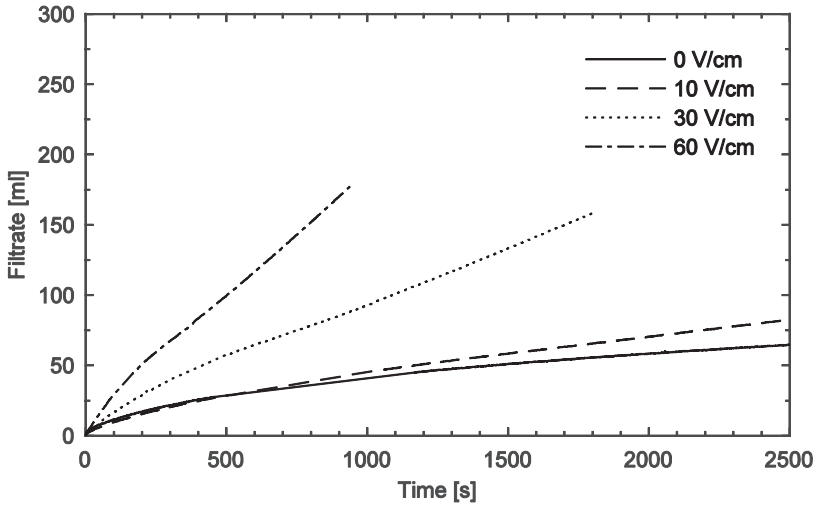

Figure 4.28. *Filtrate obtained during the electrofiltration of a buffered suspension with the addition of 0.1 g Na_2CO_3/dm^3 and a filtration pressure of 0.3 MPa.*

4.2.2.3. Power demand

The power demand for electro-assisted filtration of microcrystalline suspensions at various ionic strength is shown in Figure 4.29 at a constant applied voltage of 30 V/cm. As the ionic strength of the suspension is increased, so is the electrical conductivity of the system. A higher power demand is thus required in order to maintain a constant electric field strength. The relation between the ionic strength of the suspension and the power demand will therefore have a large influence on industrial applications of electro-assisted filtration.

The power demand in Figure 4.29 can be seen to increase during the early stage of the filtration operation, indicating that the electrical conductivity of the system increases during the electrofiltration operation. The power demand during electro-assisted filtration of buffered microcrystalline cellulose suspensions is shown in Figure 4.30. For the buffered suspensions the power demand is instead decreasing during the early stage of the electrofiltration, a result of the acidic electrolysis products consuming the buffer and lowering the electrical conductivity of the system. In the latter stages of the filtration operation the power demand, and thus the electrical conductivity, increase for the buffered suspensions as the buffer has been consumed and a pH profile is establish in the filter cell. The observed increase in the power demand during the electrofiltration operations in Figure 4.29 is thus mainly an effect of accumulation of ionic electrolysis products in the filter cell.

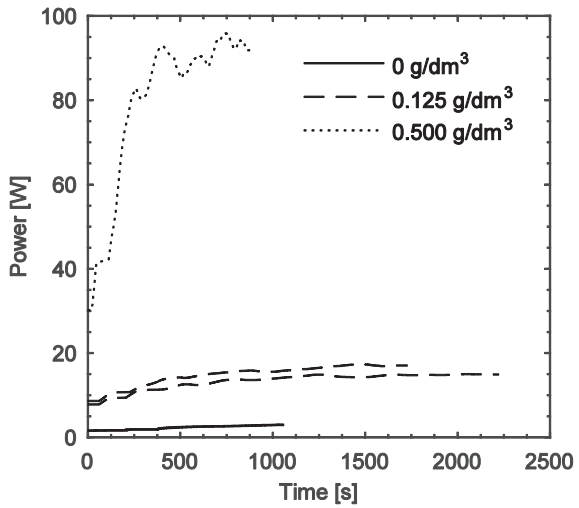

Figure 4.29. *Power demand during the electrofiltration of microcrystalline cellulose suspensions at different ionic strengths achieved by addition of $NaNO_3$. The filtration pressure applied was 0.3 MPa and the electric field 30 V/cm.*

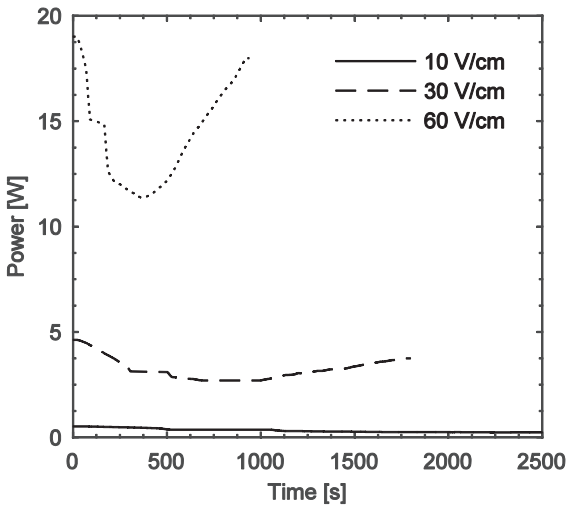

Figure 4.30. *Power demand during the electrofiltration of suspensions buffered by the addition of 0.1 g Na_2CO_3/dm^3. The filtration pressure applied was 0.3 MPa.*

4.2.2.4. Ohmic heating

The temperature in the filter cell, measured 5 mm from the filter medium during electrofiltration of microcrystalline cellulose in suspensions of different ionic strengths, is shown in Figure 4.31 for an applied voltage of 30 V/cm. The temperature rise caused by ohmic heating is influenced strongly by the ionic strength of the suspension: it is a result of the increasing power demand of the electrofiltration operation at a constant voltage as the electrical conductivity of the system is increased. The influence of the electric field strength is shown in Figure 4.32 for a microcrystalline cellulose suspension with addition of 0.5 g $NaNO_3$/dm^3. Increasing the electric field strength increases the ohmic heating. The temperature in the filter cell can also be seen to increase towards the filter medium. In electrofiltration experiments with a high ionic strength, the temperature rise in the filter cell was found to be substantial and, consequently, influences the filtration behaviour by affecting the viscosity of the fluid.

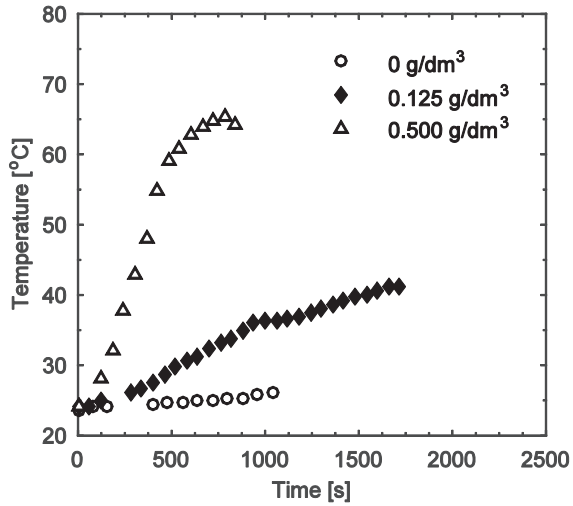

Figure 4.31. *Temperature measured 5 mm from the filter medium during the electrofiltration of microcrystalline cellulose suspensions of varying ionic strengths by addition of $NaNO_3$. The electric field applied was 30 V/cm and the filtration pressure 0.3 MPa.*

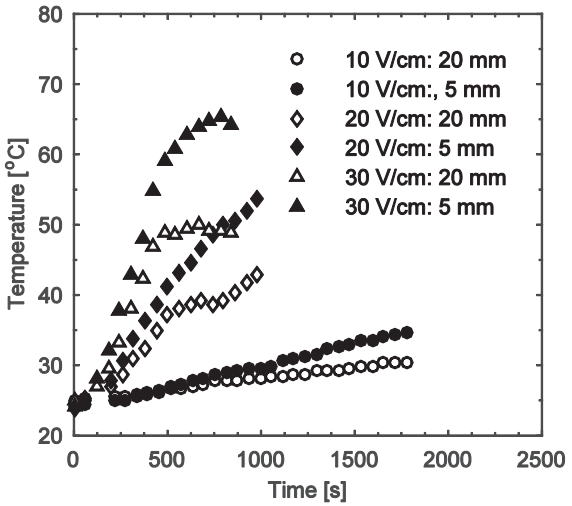

Figure 4.32. *Temperature in the filter cell during the electrofiltration of microcrystalline cellulose suspensions with the addition of 0.5 g $NaNO_3/dm^3$. The filtration pressure was 0.3 MPa.*

4.2.3. Modelling electro-assisted filtration

The way in which the electric field influenced the electro-assisted filtration of microcrystalline cellulose was described using the electrofiltration model outlined in Section 2.5. The electrofiltration model uses a number of input parameters all of which, with the exception of the apparent zeta-potential, were estimated from either literature data or filtration experiments performed without an electric field, see Table 4.5.

The model was used to describe the electrofiltration behaviour of systems with a low ionic strength in which the amount of electrolysis reactions was limited. The electrolysis reactions resulted in a pH profile between the electrodes; the pH in the filtrate was measured at 10 when the cathode was placed beneath the filter medium and 3.5 when the direction of the electric field was reversed so that the anode was beneath the filter medium. The pH profile was verified by dissecting cakes from filtration experiments aborted at different stages during the filtration operation. During the electrofiltration experiments, the cathode was placed beneath the filter medium; the pH in the filter cell was such that the particles were charged in the rate-limiting region close to the filter medium. The electrolysis reactions are therefore assumed to have no major influence on the electro-assisted filtration behaviour for the suspension conditions used in these experiments.

The input parameters of the electrofiltration model are reported in Table 4.5. The average specific filtration resistance and the filtration resistance of the filter medium were determined by pressure filtration experiments for each filtration pressure. The apparent zeta-potential was the only model parameter used to fit the model to the electrofiltration experiments; the same value was used to describe electrofiltration experiments at different filtration pressures as well

as for electroosmotic dewatering without an applied filtration pressure. The influence of the measured temperature on the filtration behaviour was included in the electrofiltration model through the temperature dependence of the viscosity of water. The increase in temperature that occurred during the electro-assisted filtration experiments at the low ionic strength in the suspension was limited, see Figure 4.31, and was not found to have a strong influence on the filtration rate.

Table 4.5. *Input parameters of the electrofiltration model.*

Filtration properties:			
Δp_H [MPa]	0	0.13	0.32
$\phi_{s,0}$ [-]	0.05	0.05	0.05
ϕ_{cake} [-]	0.30	0.30	0.30
$\alpha_{avg}c$ [m/m^3 filtrate]	-	$2.29 \cdot 10^{15}$	$2.99 \cdot 10^{15}$
R_m [m^{-1}]	-	$10.1 \cdot 10^{12}$	$8.07 \cdot 10^{12}$
Fitting parameter:			
Apparent zeta-potential [mV]	-18		

The amount of filtrate obtained during electroosmotic dewatering of the suspension without a filtration pressure being applied is shown in Figure 4.33 for two different levels of constant voltage applied. The behaviour could be described by the Helmholtz-Smoluchowski equation, with the apparent zeta-potential being the only model parameter: the fitted value is given in Table 4.5. The difference in the electroosmotic dewatering rate between the two voltages applied is described accurately during the early stages of the operation, but deviates somewhat when the electroosmotic dewatering rate decreases during the latter stages of the operation, as discussed in Section 4.2.1.

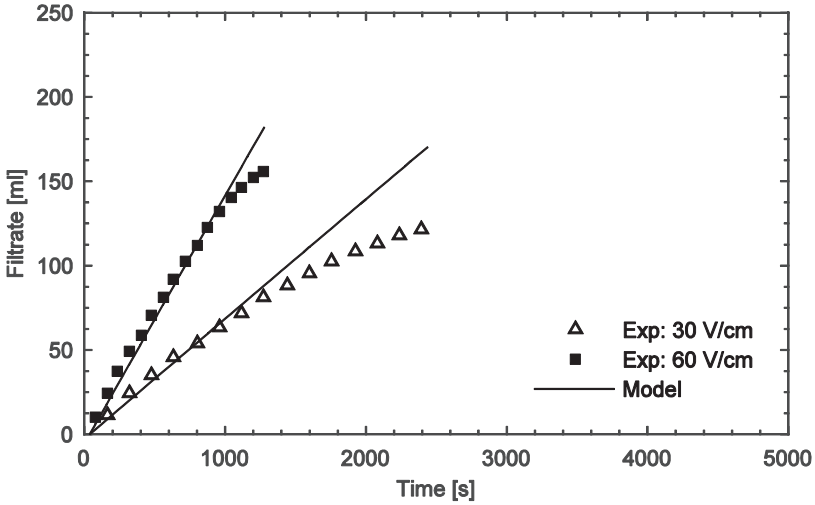

Figure 4.33. *Electroosmotic dewatering of a mechanically-treated microcrystalline suspension with pH 6.3 and low ionic strength, with different applied electric fields. The electrofiltration model is included.*

The electrofiltration model is compared with experimental measurements of the accumulated filtrate at various applied voltages at an applied filtration pressure of 0.13 MPa in Figure 4.34 and 0.32 MPa in Figure 4.35. The model gives a good description of the behaviour at different applied electric fields and filtration pressures.

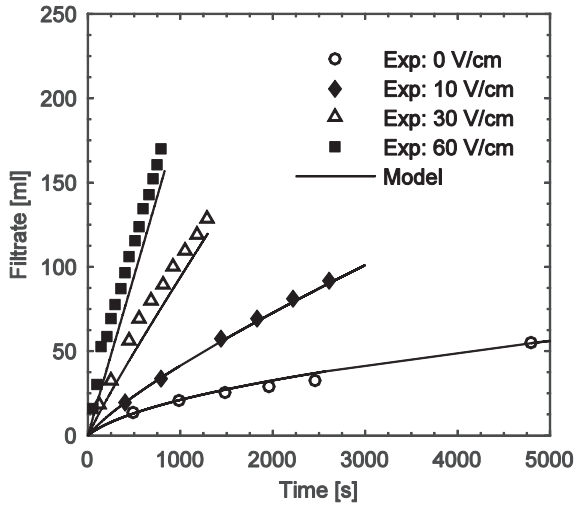

Figure 4.34. *Electrofiltration of a mechanically-treated microcrystalline cellulose suspension at pH 6.3 with an applied filtration pressure of 0.13 MPa and various levels of applied electric fields. The electrofiltration model is included.*

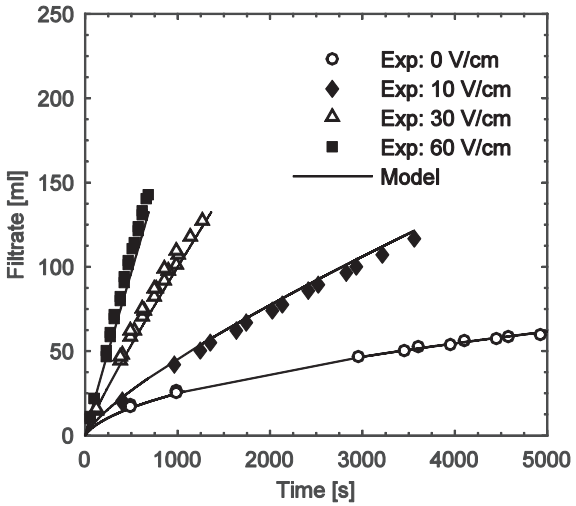

Figure 4.35. *Electrofiltration of a mechanically-treated microcrystalline cellulose suspension at pH 6.3 with an applied filtration pressure of 0.32 MPa and various levels of applied electric fields. The electrofiltration model is included.*

The height of the filter cake according to the electrofiltration model is shown in Figure 4.36 for an applied filtration pressure of 0.32 MPa. It is in good agreement with the experimental measurements of the solidosity in Figure 4.22, as the growth of the filter cake is below the measurement height of 6 mm when an electric field is applied. The contribution made by the electrophoretic force suggested by the electrofiltration model can describe the electrofiltration process even though the transition between the filter cake and the suspension is simplified in the electrofiltration model by the assumption that the filter cake is incompressible.

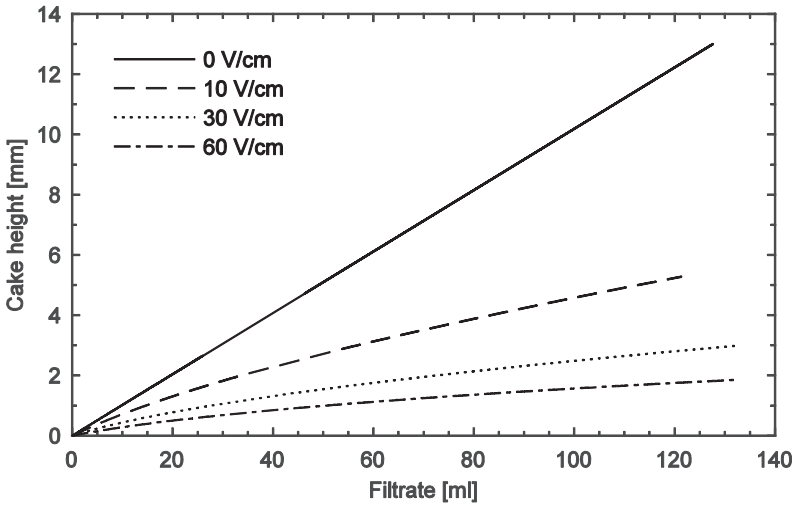

Figure 4.36. *Height of the filter cake, according to the electrofiltration model, at different applied voltages and an applied filtration pressure of 0.32 MPa.*

4.2.4. Summary of the electro-assisted filtration results

Electro-assisted filtration can be used to improve the dewatering rate of cellulosic materials with high specific surface areas. The specific surface area of the cellulosic materials studied in this thesis was not found to have a major influence on the rate of electroosmotic dewatering: the improvement obtained by electro-assisted filtration thus increases with increasing specific surface area of the solid material.

Electrolysis products formed during the electro-assisted filtration operation may influence the pH in the filter cake unless they are removed. The formation of acidic electrolysis products at the anode had a detrimental effect on the electro-assisted filtration of microcrystalline cellulose. Increasing the ionic strength of a system increased the amount of electrolysis products as well as the power demand during electro-assisted filtration to a large extent.

The influence of an electric field on the filtration behaviour of microcrystalline cellulose could be described by an electrofiltration model for systems with a low ionic strength in which the amount of electrolysis reactions was limited. The electrofiltration model was based on the average filtration properties determined from pressure filtration experiments. Only one model parameter, the apparent zeta-potential, was used to describe the influence of the electric field through electroosmosis and electrophoresis.

5. Conclusions

Electro-assisted filtration can be used to improve the dewatering rate of cellulosic materials with high specific surface areas. The specific surface area of the mechanically-modified microcrystalline cellulose particles studied in this thesis was not found to have a major influence on the rate of electroosmotic dewatering: the improvement obtained by electro-assisted filtration thus increases with increasing specific surface area of the solid material.

Increasing the ionic strength of a system increases the power demand during electro-assisted filtration. The major potential for industrial application of electro-assisted filtration is therefore for systems of limited ionic strength. The ionic strength of the system involved also influences the amount of electrolysis products that form during the filtration operation. In the case of the microcrystalline cellulose used in this study, the electrolysis products had a detrimental effect on the electro-assisted filtration behaviour by decreasing the surface charge of the solid material in the filter cake.

The surface roughness of microcrystalline cellulose particles has a large influence on the pressure filtration behaviour: a rugged particle surface increases the specific surface area subjected to drag. The filtration resistance of microcrystalline cellulose suspensions was also much higher for neutral or alkaline conditions, where the particle surfaces are charged, than at acidic conditions, where the surface charge is low. The effect is mainly a result of charged particle surfaces increasing the specific surface area subjected to drag, and not an effect of changes to the solidosity of the filter cake.

Dead-end filtration operations that are dominated by the filtration resistance of the filter cake can be described accurately by a filtration model based on experimental measurements of the local filtration properties. The use of experimental measurements of the local filtration properties allows the pressure dependence of a filtration operation to be determined from a small number of experiments.

6. Future work

The experimental work undertaken in this thesis has shown that electro-assisted filtration can be used to improve the filtration rate of cellulosic materials with high specific surface areas. Before electro-assisted filtration can be implemented successfully in biorefinery applications, however, a number of questions remain to be answered.

An improved understanding of the influence of electrophoresis on the growth of filter cakes is required if electro-assisted filtration operations are to be designed adequately and properly. While the electroosmotic dewatering rate of a system can be controlled by the strength of the electric field applied, the effect of electrophoresis is influenced by both the electric field and the filtration pressure. If the electrophoretic effect influences the formation of a filter cake in such a way that the filtration resistance of the cake is decreased, then the energy demand could be reduced to below that of operations dominated by the electroosmotic dewatering. Controlling the electro-assisted filtration operation of a system in this manner requires an understanding of how the properties of the solid material, the conditions of the suspension, the filtration pressure and the electric field combine to influence the growth of the filter cake. Experimental measurements of the properties of the filter cake, such as its height, local solidosity and local cohesive strength, could be very beneficial towards fulfilling this goal.

The power demand of electro-assisted filtration operations is influenced strongly by the electrical conductivity of the system, so the main potential industrial application is therefore for systems with a limited ionic strength. Industrial processes that include an electro-assisted dewatering step could therefore benefit from including a measure of decreasing the ionic strength of the system prior to dewatering: one interesting option here is washing with crossflow filtration. It could even be possible to employ this operation as an electro-assisted washing step, since crossflow filtration can be more effective at lower applied voltages than dead-end electro-assisted dewatering.

In the production of materials where contamination of the filter cake cannot be tolerated, the electro-assisted filtration equipment must be designed in such a way that the electrolysis products can be removed. Flushing the electrodes is a promising method, although it increases the complexity of the filtration equipment required. Identifying a suitable equipment design for the removal of the electrolysis products is a key step towards utilising electro-assisted filtration not only in traditional applications, such as sludge handling and wastewater treatment, but also in the production of materials.

7. Nomenclature

Latin letters

A	Filter area [m^2]
A_c	Cross-sectional area [m^2]
a	Radius [m]
b	Cell radius [m]
c	Mass of solids per unit of filtrate volume [kg/m^3]
D_{cap}	Hydraulic diameter of a pore [m]
d	Electrode separation [m]
d_γ	Average path length of radiation [m]
E	Electric field strength [V/m]
E_c	Electric field strength in the filter cake [V/m]
E_{cr}	Critical electric field strength [V/m]
E_s	Electric field strength in the suspension [V/m]
e	Elementary charge [C]
F	Faraday constant [C/mol]
h	Height of the filter cake [m]
I	Current [A]
I_{is}	Ionic strength [mol/m^3]
K	Permeability [m^2]
K_L	Conductivity of the bulk liquid [S/m]
K_{sys}	Conductivity of the system [S/m]
K^σ	Surface conductivity [S]
k	Kozeny-Carman constant [-]
k_B	Boltzmann constant [J/K]
k_i	Particle permeability [m^2]
N_A	Avogadro constant [mol^{-1}]
n	Empirical parameter [-]
n_p	Electrolysis products [mol]
n_γ	Number of γ-detector observations [-]
$n_{\gamma,0}$	Number of γ-detector observations for the empty filter cell [-]
P_a	Empirical parameter [Pa]
$P_{applied}$	Applied filtration pressure [Pa]
P_l	Hydrostatic pressure [Pa]
P_s	Compressive pressure [Pa]
$\dot{Q}$	Power [W]
R	Electrical resistance [Ω]
R_c	Filter cake resistance [m^{-1}]

R_m	Filter medium resistance [m^{-1}]
$R_{m,e}$	Electrical resistance of the filter medium [Ω]
S_p	Specific surface area [m^{-1}]
$S_{p,ext}$	Specific external surface area [m^{-1}]
$S_{p,i}$	Specific internal surface area [m^{-1}]
T	Temperature [K]
t	Time [s]
$U_{applied}$	Applied voltage [V]
U_{open}	Open circuit voltage [V]
u	Superficial fluid velocity relative to the solid material [m/s]
u_i	Ionic mobility of species i [m^2/sV]
V	Filtrate volume [m^3]
V_{eo}	Filtrate from electroosmosis [m^3]
V_p	Filtrate from pressure filtration [m^3]
V_{total}	Volume of the filter cake [m^3]
v	Superficial fluid velocity [m/s]
v_{cap}	Average fluid velocity in a pore [m/s]
v_d	Electromigration velocity [m/s]
v_e	Electrophoretic velocity [m/s]
v_{eo}	Electroosmotic velocity [m/s]
v_{solid}	Superficial velocity of solids [m/s]
z	Distance from the filter medium [m]
z_i	Charge number of ionic species i [-]

Greek letters

α	Specific filtration resistance [m/kg]
α_{avg}	Average specific filtration resistance [m/kg]
α_0	Empirical parameter [m/kg]
β	Empirical parameter [-]
ΔP	Pressure drop [Pa]
ΔP_c	Pressure drop over the filter cake [Pa]
Δp_E	Electroosmotic pressure [Pa]
Δp_H	Hydraulic pressure [Pa]
ε_{rs}	Relative dielectric constant of the fluid [-]
ε_0	Permittivity of vacuum [F/m]
ζ	Zeta potential [V]
κ	Reciprocal Debye length [m^{-1}]
μ	Viscosity of the fluid [Pa·s]
$\mu_{\gamma,l}$	Attenuation coefficient of the liquid phase [m^{-1}]
$\mu_{\gamma,s}$	Attenuation coefficient of the solid phase [m^{-1}]
ρ_s	Density of solid material [kg/m^3]
ϕ	Solidosity [-]
ϕ_c	Solidosity of the filter cake [-]
ϕ_i	Particle solidosity [-]
ϕ_s	Solidosity of the suspension [-]
$\phi_{s,0}$	Initial solidosity of the suspension [-]
ϕ_0	Empirical parameter [-]

8. Acknowledgements

The research presented in this thesis has been performed within the Wallenberg Wood Science Center and the financial support of the Knut and Alice Wallenberg Foundation is gratefully acknowledged.

I would like to express my gratitude to a number of people for the contribution they have made:

- First of all, my supervisor and examiner, Prof. Hans Theliander. Thank you for your enthusiasm and for giving me every opportunity to grow as a researcher.

- My incredible co-supervisor, Dr. Tuve Mattsson, for our invaluable discussions and for all the support you have given my work. It has been a privilege working with you.

- My co-author, and fellow filtration researcher, Julie Durruty.

- The talented Master's students Sandra Jonsson and Jessica Jakobsson whom I supervised during their respective diploma work. Thank you for your valuable contributions.

- Esa Väänänen, Erik Brunius and Torbjörn Jönsson, for your skilful work with the electrofiltration equipment in the workshop at the Division of Chemistry and Chemical Engineering.

- Ms. Maureen Sondell for her excellent linguistic review of this thesis as well as the articles it includes.

I would also like to thank all my colleagues, past and present, at the Department of Forest Products and Chemical Engineering at Chalmers as well as at the Wallenberg Wood Science Center. A special thank you goes to Tor Sewring and Dr. Tyrone Wells for providing daily laughs: it was a pleasure sharing an office with you. Thank you, Dr. Anna Palme, for your spirited input on both research and teaching, and thank you, Dr. Merima Hasani and Karin Sahlin, for sharing your expertise. I am also very grateful for all the support provided by Eva Kristenson and Malin Larsson in tackling administrative tasks.

Last, but not least, I am indebted to my family, friends and Augusta. Thank you for all your support!

9. References

Araki, J., Wada, M., Kuga, S., Okano, T., 1999. Influence of surface charge on viscosity behavior of cellulose microcrystal suspension. Journal of Wood Science 45, 258-261.

Atsumi, K., Akiyama, T., 1975. A study of cake filtration. Journal of Chemical Engineering of Japan 8, 487-492.

Auzerais, F.M., Jackson, R., Russel, W.B., Murphy, W.F., 1990. The transient settling of stable and flocculated dispersions. Journal of Fluid Mechanics 221, 613-639.

Barton, W., Miller, S., Veal, C., 1999. The electrodewatering of sewage sludges. Drying technology 17, 498-522.

Bergström, L., 1992. Sedimentation of Flocculated Alumina Suspensions: γ-Ray Measurements and Comparison with Model Predictions. Journal of the Chemical Society, Faraday Transactions 88, 3201-3211.

Bierck, B.R., Wells, S.A., Dick, R.I., 1988. Compressible cake filtration: monitoring cake formation and shrinkage using synchrotron X-rays. Journal (Water Pollution Control Federation) 60, 645-650.

Bowen, W.R., Jenner, F., 1995. Dynamic ultrafiltration model for charged colloidal dispersions: A Wigner-Seitz cell approach. Chemical Engineering Science 50, 1707-1736.

Brinkman, H., 1947. A calculation of the viscous force exerted by a flowing fluid on a dense swarm of particles. Applied Scientific Research 1, 27-34.

Buscall, R., White, L.R., 1987. The consolidation of concentrated suspensions. Part 1.-The theory of sedimentation. Journal of the Chemical Society, Faraday Transactions 1: Physical Chemistry in Condensed Phases 83, 873-891.

Carman, P.C., 1937. Fluid flow through granular beds. Transactions of the Institution of Chemical Engineers 15, 150-166.

Chase, G.G., Willis, M.S., 1992. Compressive cake filtration. Chemical Engineering Science 47, 1373-1381.

Citeau, M., Larue, O., Vorobiev, E., 2011. Influence of salt, pH and polyelectrolyte on the pressure electro-dewatering of sewage sludge. Water Research 45, 2167-2180.

Citeau, M., Larue, O., Vorobiev, E., 2015. Chapter Eight - Electric (Electro/Dielectro-Phoretic)—Force Field Assisted Separators A2 - Tarleton, Steve, Progress in Filtration and Separation. Academic Press, Oxford, pp. 325-397.

Citeau, M., Loginov, M., Vorobiev, E., 2016. Improvement of sludge electrodewatering by anode flushing. Drying technology 34, 307-317.

Citeau, M., Olivier, J., Mahmoud, A., Vaxelaire, J., Larue, O., Vorobiev, E., 2012. Pressurised electro-osmotic dewatering of activated and anaerobically digested sludges: Electrical variables analysis. Water Research 46, 4405-4416.

Clayton, S.A., Scholes, O.N., Hoadley, A.F.A., Wheeler, R.A., McIntosh, M.J., Huynh, D.Q., 2006. Dewatering of Biomaterials by Mechanical Thermal Expression. Drying technology 24, 819-834.

Coulson, J.M., 1949. The flow of fluids through granular beds: effect of particle shape and voids in streamline flow. Trans. Inst. Chem. Eng 27, 237-257.

Curvers, D., Maes, K.C., Saveyn, H., De Baets, B., Miller, S., Van der Meeren, P., 2007. Modelling the electro-osmotically enhanced pressure dewatering of activated sludge. Chemical Engineering Science 62, 2267-2276.

Darcy, H., 1856. Les fontaines publiques de la ville de Dijon. Victor Dalamont, Paris.

Delgado, A.V., González-Caballero, F., Hunter, R.J., Koopal, L.K., Lyklema, J., 2007. Measurement and interpretation of electrokinetic phenomena. Journal of Colloid and Interface Science 309, 194-224.

Dell, C.C., Sinha, J., 1964. The mechanism of removal of water from flocculated clay sediments. Trans. Br. Ceram. Soc. 63, 603-614.

Deo, S., 2009. Stokes Flow Past a Swarm of Deformed Porous Spheroidal Particles with Happel Boundary Condition. Journal of Porous Media 12, 347-359.

Dirckx, C.J., Clark, S.A., Hall, L.D., Antalek, B., Tooma, J., Hewitt, J.M., Kawaoka, K., 2000. Magnetic resonance imaging of the filtration process. AIChE Journal 46, 6-14.

Fathi-Najafi, M., Theliander, H., 1995. Determination of local filtration properties at constant pressure. Separations Technology 5, 165-178.

Fox, R.W., McDonald, A.T., Pritchard, P.J., 2004. Introduction to fluid mechanics, 6 ed. John Wiley & Sons New York.

Fu, L.F., Dempsey, B.A., 1998. Modeling the effect of particle size and charge on the structure of the filter cake in ultrafiltration. Journal of Membrane Science 149, 221-240.

Grace, H., 1953. Resistance and Compressibility of Filter Cakes. II. Under Conditions of Pressure Filtration. Chemical Engineering Progress 49, 367-377.

Gözke, G., Posten, C., 2010. Electrofiltration of Biopolymers. Food Engineering Reviews 2, 131-146.

Happel, J., 1958. Viscous Flow in Multiparticle Systems: Slow Motion of Fluids Relative to Beds of Spherical Particles. AIChE Journal 4, 197-201.

Haselton, W.R., 1955. Gas adsorption of wood, pulp, and paper. II. The application of gas adsorption techniques to the study of the area and structure of pulps and the unbonded and bonded area of paper. Tappi 38, 716-723.

Henry, D.C., 1931. The Cataphoresis of Suspended Particles. Part I. The Equation of Cataphoresis. Proceedings of the Royal Society of London. Series A, Containing Papers of a Mathematical and Physical Character 133, 106-129.

Henry, J.D., Lawler, L.F., Kuo, C.H.A., 1977. A solid/liquid separation process based on cross flow and electrofiltration. AIChE Journal 23, 851-859.

Hiemenz, P.C., Rajagopalan, R., 1997. Principles of Colloid and Surface Chemistry, revised and expanded. CRC press.

Hofmann, R., Käppler, T., Posten, C., 2006. Pilot-scale press electrofiltration of biopolymers. Separation and Purification Technology 51, 303-309.

Hofmann, R., Posten, C., 2003. Improvement of dead-end filtration of biopolymers with pressure electrofiltration. Chemical Engineering Science 58, 3847-3858.

Holdich, R.G., Sinclair, I., 1992. Measurement of slurry solids content by electrical conductivity. Powder Technology 72, 77-87.

Horsfield, M.A., Fordham, E.J., Hall, C., Hall, L.D., 1989. ^{1}H NMR imaging studies of filtration in colloidal suspensions. Journal of Magnetic Resonance 81, 593-596.

Hutto, F., 1957. Distribution of porosity in filter cakes. Chemical Engineering Progress 53, 328-332.

Iritani, E., Katagiri, N., Yamaguchi, K., Cho, J.-H., 2006. Compression-permeability properties of compressed bed of superabsorbent hydrogel particles. Drying technology 24, 1243-1249.

Isogai, A., 2013. Wood nanocelluloses: fundamentals and applications as new bio-based nanomaterials. Journal of Wood Science 59, 449-459.

Iwata, M., Tanaka, T., Jami, M.S., 2013. Application of Electroosmosis for Sludge Dewatering—A Review. Drying technology 31, 170-184.

Johansson, C., Theliander, H., 2003. Measuring concentration and pressure profiles in deadend filtration. Filtration 3, 114-120.

Jones, C.J.F.P., Lamont-Black, J., 2012. electrokinetic belt press apparatus and a belt therefor. Google Patents.

Joule, J.P., 1841. XXXVIII. On the heat evolved by metallic conductors of electricity, and in the cells of a battery during electrolysis. Philosophical Magazine Series 3 19, 260-277.

Ju, S., Weber, M.E., Mujumdar, A.S., 1991. Electroosmotic dewatering of bentonite suspensions. Separations Technology 1, 214-221.

Kadla, J.F., Kubo, S., Venditti, R.A., Gilbert, R.D., Compere, A.L., Griffith, W., 2002. Lignin-based carbon fibers for composite fiber applications. Carbon 40, 2913-2920.

Kilchherr, R., Koenders, M.A., Wakeman, R.J., Tarleton, E.S., 2004. Transport processes during electrowashing of filter cakes. Chemical Engineering Science 59, 1103-1114.

Kobayashi, K., Hakoda, M., Hosoda, Y., Iwata, M., Yukawa, H., 1979. Electroosmotic flow through particle beds and electroosmotic pressure distribution. Journal of Chemical Engineering of Japan 12, 492-494.

Koenders, M.A., Reymann, S., Wakeman, R.J., 2000. The intermediate stage of the dead-end filtration process. Chemical Engineering Science 55, 3715-3728.

Koenders, M.A., Wakeman, R.J., 1997. Filter Cake Formation from Structured Suspensions. Chemical Engineering Research and Design 75, 309-320.

Köhnke, T., Östlund, Å., Brelid, H., 2011. Adsorption of Arabinoxylan on Cellulosic Surfaces: Influence of Degree of Substitution and Substitution Pattern on Adsorption Characteristics. Biomacromolecules 12, 2633-2641.

Kondo, S., Suwa, T., Sano, S., Muroi, O., 1991. Compressive and electro-osmotic dehydrator. Google Patents.

Kopinga, K., Pel, L., 1994. One-dimensional scanning of moisture in porous materials with NMR. Review of Scientific Instruments 65, 3673-3681.

Kozeny, J., 1927. Über Kapillare Leitung des Wassers im Boden. Sitzungsberichte der Akademia der Wissenschaften in Wien, Mathematisch-Naturwissenschaftliche 136, 271-306.

La Heij, E.J., Kerkhof, P.J.A.M., Kopinga, K., Pel, L., 1996. Determining porosity profiles during filtration and expression of sewage sludge by NMR imaging. AIChE Journal 42, 953-959.

Landman, K.A., White, L.R., 1992. Determination of the hindered settling factor for flocculated suspensions. AIChE Journal 38, 184-192.

Landman, K.A., White, L.R., Eberl, M., 1995. Pressure filtration of flocculated suspensions. AIChE Journal 41, 1687-1700.

Larue, O., Wakeman, R.J., Tarleton, E.S., Vorobiev, E., 2006. Pressure electroosmotic dewatering with continuous removal of electrolysis products. Chemical Engineering Science 61, 4732-4740.

Larue, O., Vorobiev, E., 2004. Sedimentation and water electrolysis effects in electrofiltration of kaolin suspension. AIChE Journal 50, 3120-3133.

Lockhart, N.C., 1983a. Electroosmotic dewatering of clays, III. Influence of clay type, exchangeable cations, and electrode materials. Colloids and Surfaces 6, 253-269.

Lockhart, N.C., 1983b. Electroosmotic dewatering of clays. II. Influence of salt, acid and flocculants. Colloids and Surfaces 6, 239-251.

Loginov, M., Citeau, M., Lebovka, N., Vorobiev, E., 2013. Electro-dewatering of drilling sludge with liming and electrode heating. Separation and Purification Technology 104, 89-99.

Luukkonen, P., Maloney, T., Rantanen, J., Paulapuro, H., Yliruusi, J., 2001. Microcrystalline Cellulose-Water Interaction—A Novel Approach Using Thermoporosimetry. Pharmaceutical Research 18, 1562-1569.

Lyklema, J., 1995. 4 - Electrokinetics and Related Phenomena, in: Lyklema, J. (Ed.), Fundamentals of Interface and Colloid Science. Academic Press, pp. 4-1-4-135.

Mahmoud, A., Olivier, J., Vaxelaire, J., Hoadley, A.F.A., 2010. Electrical field: A historical review of its application and contributions in wastewater sludge dewatering. Water Research 44, 2381-2407.

Mahmoud, A., Olivier, J., Vaxelaire, J., Hoadley, A.F.A., 2011. Electro-dewatering of wastewater sludge: Influence of the operating conditions and their interactions effects. Water Research 45, 2795-2810.

Mattsson, T., Sedin, M., Theliander, H., 2012. On the local filtration properties of microcrystalline cellulose during dead-end filtration. Chemical Engineering Science 72, 51-60.

Meeten, G.H., 1993. A dissection method for analysing filter cakes. Chemical Engineering Science 48, 2391-2398.

Miller, S.A., Johnston, B.K., Veal, C., 2005. Apparatus for electrodewatering. Google Patents.

Moulik, S.P., 1971. Physical aspects of electrofiltration. Environmental Science & Technology 5, 771-776.

Muralidhara, H.S., Ensminger, D., Putnam, A., 1985. Acoustic dewatering and drying (low and high frequency): state of the art review. Drying technology 3, 529-566.

Navab-Daneshmand, T., Beton, R., Hill, R.J., Frigon, D., 2015. Impact of joule heating and ph on biosolids electro-dewatering. Environmental Science and Technology 49, 5417-5424.

Okamura, S., Shirato, M., 1955. Liquid Pressure Distribution within Cakes in the Constant Pressure Filtration. Chemical Engineering (Japan) 19, 104-110.

Oksman, K., Aitomäki, Y., Mathew, A.P., Siqueira, G., Zhou, Q., Butylina, S., Tanpichai, S., Zhou, X., Hooshmand, S., 2016. Review of the recent developments in cellulose nanocomposite processing. Composites Part A: Applied Science and Manufacturing 83, 2-18.

Olivier, J., Conrardy, J.-B., Mahmoud, A., Vaxelaire, J., 2015. Electro-dewatering of wastewater sludge: An investigation of the relationship between filtrate flow rate and electric current. Water Research 82, 66-77.

Raats, M.H.M., van Diemen, A.J.G., Lavèn, J., Stein, H.N., 2002. Full scale electrokinetic dewatering of waste sludge. Colloids and Surfaces A: Physicochemical and Engineering Aspects 210, 231-241.

Rabie, H.R., Mujumdar, A.S., Weber, M.E., 1994. Interrupted electroosmotic dewatering of clay suspensions. Separations Technology 4, 38-46.

Ragauskas, A.J., Williams, C.K., Davison, B.H., Britovsek, G., Cairney, J., Eckert, C.A., Frederick, W.J., Hallett, J.P., Leak, D.J., Liotta, C.L., Mielenz, J.R., Murphy, R., Templer, R., Tschaplinski, T., 2006. The Path Forward for Biofuels and Biomaterials. Science 311, 484-489.

Rice, C.L., Whitehead, R., 1965. Electrokinetic Flow in a Narrow Cylindrical Capillary. The Journal of Physical Chemistry 69, 4017-4024.

Rietema, K., 1953. Stabilizing effects in compressible filter cakes. Chemical Engineering Science 2, 88-94.

Ruth, B.F., 1935. Studies in Filtration III. Derivation of General Filtration Equations. Industrial & Engineering Chemistry 27, 708-723.

Ruth, B.F., 1946. Correlating Filtration Theory with Industrial Practice. Industrial & Engineering Chemistry 38, 564-571.

Saveyn, H., Curvers, D., Pel, L., De Bondt, P., Van der Meeren, P., 2006. In situ determination of solidosity profiles during activated sludge electrodewatering. Water Research 40, 2135-2142.

Saveyn, H., Van der Meeren, P., Hofmann, R., Stahl, W., 2005. Modelling two-sided electrofiltration of quartz suspensions: Importance of electrochemical reactions. Chemical Engineering Science 60, 6768-6779.

Schäfer, B., Hecht, M., Harting, J., Nirschl, H., 2010. Agglomeration and filtration of colloidal suspensions with DVLO interactions in simulation and experiment. Journal of Colloid and Interface Science 349, 186-195.

Sedin, P., Johansson, C., Theliander, H., 2003. On the Measurement and Evaluation of Pressure and Solidosity in Filtration. Chemical Engineering Research and Design 81, 1393-1405.

Shen, C., Russel, W.B., Auzerais, F.M., 1994. Colloidal gel filtration: Experiment and theory. AIChE Journal 40, 1876-1891.

Shirato, M., Aragaki, T., Ichimura, K., Ootsuji, N., 1971. Porosity variation in filter cake under constant-pressure filtration. Journal of Chemical Engineering of Japan 4, 172-177.

Shirato, M., Aragaki, T., Mori, R., Sawamoto, K., 1968. Predictions of constant pressure and constant rate filtrations based upon an approximate correction for side wall friction in compression permeability cell data. Journal of Chemical Engineering of Japan 1, 86-90.

Shirato, M., Sambuichi, M., Kato, H., Aragaki, T., 1969. Internal flow mechanism in filter cakes. AIChE Journal 15, 405-409.

Siró, I., Plackett, D., 2010. Microfibrillated cellulose and new nanocomposite materials: a review. Cellulose 17, 459-494.

Smiles, D.E., 1970. A theory of constant pressure filtration. Chemical Engineering Science 25, 985-996.

Smythe, M.C., Wakeman, R.J., 2000. The use of acoustic fields as a filtration and dewatering aid. Ultrasonics 38, 657-661.

Stickland, A.D., Buscall, R., 2009. Whither compressional rheology? Journal of Non-Newtonian Fluid Mechanics 157, 151-157.

Stolarski, M., Fuchs, B., Bogale Kassa, S., Eichholz, C., Nirschl, H., 2006. Magnetic field enhanced press-filtration. Chemical Engineering Science 61, 6395-6403.

Stone, J.E., Scallan, A.M., 1965. A study of cell wall structure by nitrogen adsorption. Pulp and Paper Research Institute of Canada 66, T407-T414.

Tanaka, T., Fujihara, K., Jami, M.S., Iwata, M., 2014. Constant-current electroosmotic dewatering of superabsorbent hydrogel. Colloids and Surfaces A: Physicochemical and Engineering Aspects 440, 116-121.

Tarleton, E.S., 1992. The role of Field-assisted techniques in solid/liquid separation. Filtration & Separation 29, 246-238.

Teoh, S., Tan, R.B., Tien, C., 2002. Correlation of C–P cell and filtration test data using a new test cell. Separation and Purification Technology 29, 131-139.

Tien, C., Ramarao, B.V., 2013. Can filter cake porosity be estimated based on the Kozeny–Carman equation? Powder Technology 237, 233-240.

Tiller, F.M., 1953. The role of porosity in filtration. Numerical methods for constant-rate and constant-pressure filtration based on Kozeny's law. Chemical Engineering Progress 49, 467-479.

Tiller, F.M., 1955. The role of porosity in filtration. Part 2. Analytical equations for constant rate filtration. Chem. Eng. Progr. 51.

Tiller, F.M., Cooper, H.R., 1960. The role of porosity in filtration: IV. Constant pressure filtration. AIChE Journal 6, 595-601.

Tiller, F.M., Haynes, S., Lu, W.-M., 1972. The role of porosity in filtration VII effect of side-wall friction in compression-permeability cells. AIChE Journal 18, 13-20.

Tiller, F.M., Hsyung, N.B., Cong, D.Z., 1995. Role of porosity in filtration: XII. Filtration with sedimentation. AIChE Journal 41, 1153-1164.

Tiller, F.M., Leu, W.F., 1980. Basic data fitting in filtration. Journal of the Chinese Institute of Chemical Engineers 11, 61-70.

Tiller, F.M., Lu, W.-M., 1972. The role of porosity in filtration VIII: Cake nonuniformity in compression–permeability cells. AIChE Journal 18, 569-572.

Tosun, I., 1986. Formulation of cake filtration. Chemical Engineering Science 41, 2563-2568.

Wakeman, R., 1978. A numerical integration of the differential equations describing the formation of and flow in compressible filter cakes. Trans. Inst. Chem. Eng 56, 258-265.

Wakeman, R., 1982. Effects of solids concentration and pH on electrofiltration. Filtration and separation 19, 316.

Wakeman, R.J., 1981. The formation and properties of apparently incompressible filter cakes under vacuum on downward facing surfaces. Trans. I. Chem. Eng. 59, 260-270.

Wakeman, R.J., Tarleton, E.S., 1987. Membrane fouling prevention in crossflow microfiltration by the use of electric fields. Chemical Engineering Science 42, 829-842.

van Heiningen, A., 2006. Converting a kraft pulp mill into an integrated forest biorefinery. Pulp & Paper Canada 107, 38-43.

Weber, K., Stahl, W., 2002. Improvement of filtration kinetics by pressure electrofiltration. Separation and Purification Technology 26, 69-80.

Wetterling, J., Mattsson, T., Theliander, H., 2017. Modelling filtration processes from local filtration properties: the effect of surface properties on microcrystalline cellulose. Chemical Engineering Science

Vijh, A.K., 1999. Electroosmotic dewatering (EOD) of clays and suspensions: components of voltage in an electroosmotic cell. Drying technology 17, 565-574.

Yamaguchi, M., Nakagawa, M., Ohanamori, H., Yoshida, M., Arai, T., Matsushita, H., 1993. Electroosmotic dewaterer. Google Patents.

Yim, S.S., Song, Y.M., 2008. Porosity distribution in highly compressible cake: Experimental and theoretical verification of the dense skin. Korean Journal of Chemical Engineering 25, 1524-1531.

Yoshida, H., Kitajyo, K., Nakayama, M., 1999. Electroosmotic dewatering under A.C. electric field with periodic reversals of elctrode polarity. Drying technology 17, 539-554.

Young, G.J., 1911. Slime-Filtration. Transactions of the American Institute of Mining Engineers 42, 752-784.

Yu, J.-W., Neretnieks, I., 1996. Modelling of transport and reaction processes in a porous medium in an electrical field. Chemical Engineering Science 51, 4355-4368.

Yu, X., Zhang, S., Xu, H., Zheng, L., LÜ, X., Ma, D., 2010. Influence of Filter Cloth on the Cathode on the Electroosmotic Dewatering of Activated Sludge. Chinese Journal of Chemical Engineering 18, 562-568.

Yukawa, H., Chigira, H., Hoshino, T., Iwata, M., 1971. Fundamental study of electroosmotic filtration. Journal of Chemical Engineering of Japan 4, 370-376.

Yukawa, H., Kobayashi, K., Tsukuf, Y., Yamano, S., Iwata, M., 1976. Analysis of batch electrokinetic filtration. Journal of Chemical Engineering of Japan 9, 396-401.